The effect of pH and nitrite on the haem pocket of GLB-33, a globin-coupled neuronal transmembrane receptor of *Caenorhabditis elegans*

Niels Van Brempt[a,b], Roberta Sgammato[a], Quinten Beirinckx[a,1], Dietmar Hammerschmid[b,2], Frank Sobott[a,3], Sylvia Dewilde[b,‡], Luc Moens[b], Wouter Herrebout[a], Christian Johannessen[a], and Sabine Van Doorslaer[a,*]

[a] Department of Chemistry, University of Antwerp, 2610 Antwerp, Belgium

[b] Department of Biomedical Sciences, University of Antwerp, 2610 Antwerp, Belgium

[*]Corresponding author: sabine.vandoorslaer@uantwerpen.be
[1]Current address: imec-VisionLab, Department of Physics, University of Antwerp, Belgium
[2]Current address: Department of Chemistry, King's College London, London SE1 1 DB, United Kingdom
[3]Current address: Astbury Centre for Structural Molecular Biology and School of Molecular and Cellular Biology, University of Leeds, Leeds LS2 9JT, United Kingdom
[‡]passed away on 3rd October 2020

Abstract

Out of the 34 globins in *Caenorhabditis elegans*, GLB-33 is a putative globin-coupled transmembrane receptor with a yet unknown function. The globin domain (GD) contains a particularly hydrophobic haem pocket, that rapidly oxidizes to a low-spin hydroxide ligated haem state at physiological pH. Moreover, the GD has one of the fastest nitrite reductase activity ever reported for globins. Here, we use a combination of electronic circular dichroism, resonance Raman and electron paramagnetic resonance (EPR) spectroscopy with mass spectrometry to study the pH dependence of the ferric form of the recombinantly over-expressed GD in the presence and absence of nitrite. The competitive binding of nitrite and hydroxide is examined as well as nitrite-induced haem modifications at acidic pH. Comparison of the spectroscopic results with data from other haem proteins allows to deduce the important effect of Arg at position E10 in stabilization of exogenous ligands. Furthermore, continuous-wave and pulsed EPR indicate that ligation of nitrite occurs in a nitrito mode at pH 5.0 and above. At pH 4.0, an additional formation of a nitro-bound haem form is observed along with fast formation of a nitri-globin.

Keywords

Globin; Electron paramagnetic resonance; Resonance Raman spectroscopy; *C. elegans*; Ligand binding

Abbreviations

5c: five-coordinate; 6c: 6-coordinate; Abs: absorption; Cld: chlorite dismutase; (CW) EPR: (continuous wave) electron paramagnetic resonance; ECD: electronic circular dichroism; ESE: electron spin echo; ESEEM: electron spin echo envelope modulation ; ESI: electron spray ionization; GD: globin domain; GLB-33GDΔCys: globin domain of GLB-33 C40S/C55S variant from *C. elegans*; Hb: haemoglobin; HS: high spin; HYSCORE: hyperfine sublevel correlation

spectroscopy; LS: low spin; Mb: myoglobin; NiR: nitrite reductase; NP: nitrophorin; RNS: reactive nitrogen species; ROS: reactive oxygen species; rRaman: resonance Raman; SD: single domain;

1. Introduction

Globins are small haem-containing α-helical globular proteins widespread throughout the kingdoms of life [1,2]. Besides the well-known role of globins in the O_2 transport and storage in vertebrates, globins are shown or hypothesized to be involved in a large variety of biochemical processes, including scavenging of ROS (reactive oxygen species) and RNS (reactive nitrogen species), redox reactions and ligand (*e.g.* O_2) sensing [1]. Based on their lineage, globins are classified into three families: myoglobin-like (M), sensor (S) and truncated globin (T) family [1,2,4,5]. Next to single-domain (SD) proteins, consisting of a globin protein only, chimeric proteins consisting of a globin domain (GD) coupled to other domains, such as a transmitter domain, have been identified [1,2]. The classical globin fold, with myoglobin as archetypical example, consists of eight α-helices, labelled A to H from N- to C-terminus, that are organized in a 3-over-3 (3/3) sandwich, with the haem group situated in the hydrophobic centre and the haem iron coordinated at the proximal side to the conserved His at position 8 of the F helix (F8His). This fold is found in the M and S families, with variation in this structure mainly occurring by N- and C-terminal extension and variation in length of the inter-helical segments [3]. Furthermore, globins from the T family are shorter, exhibiting the 2-over-2 globin fold (2/2), *i.e.* an α-helical sandwich of the B-E and G-H helices. They are normally shorter than the 3/3 globins and therefore indicated as truncated haemoglobins (Hbs) [6].

Caenorhabditis elegans is found to be exceptionally rich in globins and thus offers an ideal system to unravel the diversity of globin functions and globin structures. In distinct cell types of this species, 34 globin-like proteins are transcribed and expressed [7,8]. Some of these globins have been partially characterized and putative functions have been ascribed to them [9-16]. GLB-33 is the largest of the *C. elegans* globins and consists of a GD and a 7 α-helical transmembrane domain, typical for G-protein-coupled receptors. Homology modelling predicts that the GD has the classical globin fold with eight α-helices in a canonical 3/3 sandwich [16]. Similar to myoglobin (Mb), the haem iron of GLB-33GD has no distal ligand in its reduced ferrous form (so-called pentacoordination of the haem iron). However, this form oxidizes fast, resulting in a ferric haem iron that is ligated to hydroxide in a broad range of slightly acidic to basic conditions [16]. This is in contrast with the majority of other globins in which distal OH^- ligation only sets in at alkaline pH. To our knowledge, only the truncated haemoglobins of *Thermobifida fusca* (*Tf*-TrHbs) show

a similar pH-dependent behaviour [17]. Hydrogen-bonding networks with distal haem-pocket amino-acid residues are thought to stabilize the ligation of hydroxide at physiological pH [17,18]. Whereas the *in vivo* function of GLB-33 is unclear, *in vitro* experiments show that the GD reduces nitrite to NO 10x faster than Mb [16]. NO_2^- is a precursor of RNS and has been linked to cellular signalling, intestinal relaxation, vasodilation, neurotransmission, and neuromodulation in a broad range of species [19,20]. Many globins have been indicated to play a role as NO scavengers or nitrite reductases (NiRs) [19-25]. Moreover, many other haem proteins are involved in nitric-oxide pathways in different organisms and function as NO generators or deliverers, or convert nitrite to other reactive nitrogen species [21,26], suggesting the involvement of the full-length GLB-33 protein in the NO metabolism of *C. elegans*.

The globin-nitrite interaction is complex with many intermediates identified *in vitro* depending on the initial haem-iron state (Fe(III), Fe(II), Fe(II)-O_2, ...). Under specific conditions, haem modifications and partial haem loss have been observed [27-30]. After entering the haem pocket, NO_2^- can coordinate the iron ion in either the favoured N-linked nitro (—NOO) and the less favoured O-linked nitrito (—ONO) ligation mode (see Figure S1A,B for representation), which has implications for the subsequent NiR mechanism [30-34]. In the nitro mode, a formal double protonation of one of the nitrite O-atoms precedes the release of a water molecule and generation of an Fe(III)-NO species, which then dissociates. In the O-linked nitrito mode, NO is released through an ON-O bond homolysis after protonation of the iron-bonded nitrite oxygen atom, resulting in NO and an Fe(III)-hydroxo complex [31].

In this work, optical and magnetic-resonance methods are combined with native mass spectrometry (MS) to study the pH-dependent distal haem ligation, haem modifications and overall stability of the ferric form of the GLB-33GDΔCys variant in the absence and presence of nitrite. More specifically, continuous-wave (CW) and pulsed electron paramagnetic resonance (EPR) techniques, resonance Raman (rRaman), UV/Vis absorption (Abs) and electronic circular dichroism (ECD) spectroscopy are used, since they are excellent complementary tools to probe the interaction of haem proteins with various ligands [35-37]. EPR is also used to study the nitrosylated ferrous form of the protein that appears during NiR activity in the presence of a reducing agent. The GLB-33GDΔCys variant was taken such as to prevent unspecific *in vitro* multimerization of the protein at the higher protein concentrations needed for EPR.

2. Materials and Methods

2.1. Expression and purification

The cDNA coding for GLB-33GD and double mutant C40S/C55S (GLB-33GDΔCys) (glb-33 gd, bp 1120 to 1629) was cloned into a pET23a vector with a C-terminal His-tag (Novagen) using NdeI and XhoI restriction enzymes (Biolabs) as described elsewhere [16]. After growing BL21(DE3)PlysS with coding cDNA, cells were resuspended (50 mM Tris at pH 7.5, 300 mM NaCl) followed by repeated freeze-thaw cycles and sonication to lyse the cells. After centrifugation (10 min., 10000 g, 4ºC), the supernatant was loaded onto a Ni Sepharose High Performance column (GE Healthcare), pre-equilibrated with equilibration buffer (50 mM Tris-HCl at pH 7.5, 300 mM NaCl, 20 mM imidazole) and eluted (50 mM Tris at pH 7.5, 250 mM imidazole). The eluate was dialyzed with a solution of 50 mM Tris at pH 7.5, 0.5 mM Ethylenediaminetetraacetic acid (EDTA), 150 mM NaCl, and then concentrated and loaded onto a G75 gelfiltration self-packed column as a final purification step. The validity of using the variant was tested by comparing the UV-Vis and some EPR spectra of GLB-33GD and GLB-33GDΔCys at neutral pH. The GLB-33GDΔCys variant is preferred to prevent formation of intermolecular disulphide bridges at the higher protein concentrations used in EPR.
Horse skeletal muscle Mb (hsMb) was purchased from Merck KGaA (Darmstadt, Germany) and dissolved in the same buffers as GLB-33GDΔCys or explicitly stated otherwise.

2.2. UV-Vis absorption and electronic circular dichroism spectroscopy

UV-visible Abs/ECD spectra of GLB-33GDΔCys were recorded on a Chirascan®-Plus spectrophotometer (Applied Photophysics, Leatherhead, Surrey, UK). The instrument was continuously flushed with nitrogen gas (4 L/min flow rate), and the measurements were carried out at 20ºC. For all the recorded spectra, 0.2 cm path length SUPRASIL quartz sample cells (Hellma BeNeLux, Kruibeke, BE) were used. The final spectra were subtracted by the corresponding spectrum of the solvent used for the respective measurement (Tris-HCl for pH 7.5 and 6, or sodium acetate buffer for pH 5.0 and 4.0, in presence of 100 mM NaCl). The globin concentration was estimated using the absorption at the Soret peak (412 nm), and the extinction coefficient value of human neuroglobin ε_{412nm} = 130 000 $M^{-1}cm^{-1}$ [38]. 2.5 μM GLB-33GDΔCys

was measured in the spectral range between 260 and 800 nm and between 195 and 260 nm (3 s nm^{-1}, 1 nm bandwidth). All buffer exchanges were obtained via Micro Bio-Spin chromatography columns (BioRad, Hercules, California, US). Nitrite solutions were freshly prepared *prior* to each measurement.

2.3. Resonance Raman spectroscopy

rRaman spectroscopy was carried out at room temperature using a ChiralRaman-2X spectrometer (BioTools, Inc., Jupiter, Florida, USA). Unpolarised rRaman spectra were recorded in backscattering geometry, using a green laser beam from a frequency-doubled Nd:YVO_4 laser (532 nm). The instrument was running at a spectral resolution of 7 cm^{-1}. 60 μL sample was centrifuged at 14000 rpm for 5 min, at 4ºC prior to each measurement, and then loaded into 3x4x10 mm quartz cuvette (Starna Scientific Ltd, Ilford, London, UK). The laser power was set at 0.3 W at the source, and the samples were illuminated in stretches of 2 s to prevent them from heating up. The total acquisition time varied depending on the sample stability. The protein sample, prepared in sodium acetate or Trizma® hydrochloride buffer in presence of 100 mM NaCl and having final molar concentration of 25 μM, was measured in the as-purified form and upon incubation with nitrite in one to fifty molar ratio, at pH 5.0 or 7.5, respectively. Raman spectra of the samples were subtracted by the corresponding spectrum of the solvent and subsequently baseline corrected according to the Eilers-Boelens procedure [39]. For experiments with the isotopically labelled ligand, $Na^{15}NO_2$ (95 atom %) as well as $Na^{14}NO_2$ were purchased from Merck KGaA (Darmstadt, Germany).

2.4. Electron paramagnetic resonance

Globin solutions were diluted in glycerol until a final concentration of 10-25 % (v/v) glycerol. The X-band continuous wave (CW) EPR measurements were performed on an ESP300E (Bruker) spectrometer with a microwave frequency of 9.45 GHz equipped with a gas-flow cryogenic system (Oxford Instruments), allowing for operation from room temperature down to 2.5 K. The magnetic field was measured with a Bruker ER035M NMR Gauss meter. Paramagnetic O_2 was removed from the sample *via* several freeze-pump-thaw cycles. The spectra were measured with a

modulation frequency of 100 kHz and a modulation amplitude of 0.5 mT unless stated otherwise. The microwave power is mentioned in the corresponding figure captions.

X-band pulsed EPR measurements were conducted on a Bruker E580 Elexsys spectrometer (microwave frequency ≈ 9.74 GHz) equipped with an Oxford Instruments gas-flow cryogenic system to obtain an operating temperature of 6.5 K. A shot repetition time of 1 ms was used in all experiments. X-band electron-spin-echo (ESE)-detected EPR experiments [40] were recorded using the 2-pulse sequence $\pi/2$-τ-π-τ-*echo*, with pulse lengths $t_{\pi/2}$ = 16 ns and t_{π} = 32 ns and the inter-pulse distance τ varied from 96 to 4184 ns in steps of 8 ns. The X-band three-pulse ESEEM (electron spin echo envelope modulation) experiments [40] were done using a $\pi/2$-τ-$\pi/2$-T-$\pi/2$-τ-*echo* microwave pulse sequence with pulse lengths of $t_{\pi/2}$ = 16 ns and are the sum of spectra recorded at 10 τ-values in the range of 96-240 ns in steps of 16 ns with T varied from 96 ns to 4880 ns in steps of 16 ns. HYSCORE (hyperfine sublevel correlation) spectra [41] were recorded using the microwave pulse sequence $\pi/2$-τ-$\pi/2$-t_1-π-t_2-$\pi/2$-τ-*echo* with $t_{\pi/2}$ = 16 ns and t_{π} = 32 ns and t_1 and t_2 were varied from 96 ns to 4480 ns in steps of 16 ns. HYSCORE measurements were recorded with different τ-values and added together as indicated in the figure captions.

All spectral treatment and analysis were done using MATLAB (R2020a, MathWorks, USA). The three-pulse ESEEM and HYSCORE spectra were baseline-corrected using a third-order polynomial, apodized with a Hamming window and zero-filled. After Fourier transformation, the absolute-value spectra were calculated. All EPR spectra were computer simulated using EasySpin package (v.5.2.28) [42], a toolbox for MATLAB.

2.5. Mass spectrometry

GLB-33GDΔCys (20 μM) was incubated with 50-fold molar excess of $NaNO_2$ (1 mM) at pH 4.0 (50 mM sodium acetate) and pH 7.5 (50 mM Tris-HCl) for 24 hours at room temperature. After $NaNO_2$ treatment, the samples were buffer exchanged to a volatile ammonium acetate solution (100 mM, pH 6.8) using P-6 Micro Bio-Spin columns (Bio-Rad). Each sample was loaded into homemade gold-coated borosilicate glass capillaries and mounted onto a Synapt G2 HDMS mass spectrometer (Waters, Wilmslow, UK), where native nano-electrospray (ESI) ionization mass spectrometry experiments were performed. The following instrument parameters were carefully optimized to avoid ion activation and protein unfolding (Ion mobility mode): capillary voltage: 1.2

kV, sampling cone: 25 V, extractor cone: 3V, trap collision energy: 10 V, trap DC bias: 45 V, and transfer collision energy: 2 V. Pressures were set to 3.8 mbar in the source region (backing), 2.7 x 10^{-2} mbar in both trap and transfer collision cells (collision gas: Ar), and 3.0 mbar in the IMS cell. Spectra were also acquired under elevated trap collision energies (50V) to cause protein unfolding and the release of the prosthetic haem group.

3. Results

Some of the key amino-acid residues in the haem pocket of globins are, besides the conserved His at position 8 of the F-helix, the residues at positions B10, E7, and E11 (Figure S1). In a large amount of the globins, a His residue is found at position E7 (Figure S1), but this is an Ile residue in GLB-33GD [16]. Moreover, homology modelling of GLB-33GD places two Ile residues (E7, E11), Leu (CD3) and Ala(B10) near the haem on the distal side, leading to an unusually hydrophobic distal haem pocket [16]. Furthermore, on position E10 an Arg residue is found, while this is Val in horse heart myoglobin (hhMb). Research on the double mutant H64V/V67R hhMb (mutating the residues at positions E7 and E10) has shown that Arg plays an important role in directing the ligation of nitrite in the haem pocket [43]. In view of the high NiR activity of GLB-33GD and the alkaline transition at unusual low pH, we here investigate spectroscopically the pH dependence of ferric GLB-33GD and its nitrite ligation in relation to its haem-pocket structure. Also the EPR spectrum of the NO-ligated ferrous form (the final product from the NiR reaction) is considered. In the discussion section, all data will be compared to that of other haem proteins in order to understand the important role of Arg(E10).

3.1. pH dependence of ferric GLB33GD

Figure 1A (top) depicts the UV/Vis Abs spectra of ferric GLB-33GDΔCys at pH values 4.0, 5.0, 6.2 and 7.5. These spectra show that ferric GLB-33GDΔCys changes from a high-spin (*S*=5/2) ferric haem form (potentially with distal water ligation to the haem iron) at low pH to a hydroxo-ligated ferric haem form at neutral pH, in agreement with earlier findings on GLB-33GD as reported by some of us [16]. This transition can be deduced from the red shift of the Soret band

from 406 to 413 nm upon pH increase and the concomitant drastic change of the spectrum in the green-to-red range (Q bands). At low pH, a Q band appears at 502 nm with a charge-transfer band at 636 nm, which is characteristic of a 6-coordinated high-spin haem iron (6c/HS), while at neutral pH, the Q_β and Q_α bands are situated at 544 and 577 nm, respectively, with a small shoulder at ~595 nm. The latter spectrum agrees with a hexacoordination of haem iron in a low-spin state (6c/LS), such as found for the distal hydroxo-ligation of the ferric haem.

The simultaneously collected ECD spectra (Fig. 1A, bottom) exhibit positive and negative Soret ellipticity with the maxima corresponding to the respective Soret absorption bands and with minima at 362 nm and 439 nm. Under the acidic buffer conditions, the ECD spectra are reduced in Soret ellipticity, with only positive features remaining in the 300-700 nm range. The two broad CD bands, observed at 584 and 611 nm in the spectrum of ferric GLB-33GDΔCys at pH 7.5, are absent at low pH in agreement with the changes observed in the Q-bands of the UV-vis Abs spectra. The haem optical activity has been ascribed to the interaction of the haem with aromatic amino-acid residues of the globin [44]. However, the sign of the Soret ECD band of haem proteins has also been shown to be influenced by the haem insertion [44-46] and the interaction of the haem side chains, particularly the propionate side chains, with the protein matrix [44] and by the in-plane and out-of-plane deformations of the haem group [47]. ^{1}H NMR studies have revealed haem rotational disorder in both reconstituted globins and globins produced in *E. coli* [48] with a related strong change of the Soret ECD band [46]. The positive sign of the Soret ECD peak of ferric GLB33-GD at low pH agrees with what has been reported for aquomet myoglobin with a correctly inserted haem [44]. The appearance of the minima at 362 nm and 439 nm in the ECD spectra at higher pH are therefore not linked to a reversed haem insertion since only a buffer exchange was done, but can be related to the change in the spin state (HS→LS) and/or small conformational changes in the haem pocket and/or haem ruffling and saddling [47]. Finally, the ECD spectra in the far UV (Figure S2, supplementary material) show that the appearance of the aquomet form at the lowest pH is not accompanied with drastic changes in the secondary structure of the protein.

In agreement with the UV/Vis Abs data, the spin-state rRaman marker bands indicate the presence of a 6c/LS Fe(III) species at pH 7.5 (ν_3 = 1506 cm^{-1}), while a significant contribution of a 6c/HS state appears at pH 5.0 (ν_3 = 1470 cm^{-1}) with only a small residual contribution of a 6c/LS state (Fig. 1B) [16,50,50]. The oxidation marker (ν_4 = 1376 cm^{-1}) does not change and is in agreement with the ferric state.

In the absence of any hydrogen bond, the ν(Fe-OH) stretching mode is typically found around 550 cm^{-1} for 6c/LS hydroxo-haem species, while the wavenumber of this mode decreases with increasing H-bond strength [17,49,51,52]. This is illustrated by a combined rRaman and molecular dynamics study on *Tf*-TrHb, which revealed that the unusually low ν(Fe-OH) value found in this protein (489 cm^{-1}) is due to presence of strong hydrogen-bonding Trp and Tyr residues in the haem pocket [17,52]. No clear signal is observed around 550 cm^{-1} in the low-wavenumber region of the rRaman spectrum of ferric GLB-33GDΔCys at pH 7.5 (Fig. 1C). Instead, a dominant composite signal is found around 487 cm^{-1}, indicating a ν(Fe-OH) mode << 550 cm^{-1} and hence significant hydrogen bonding of the hydroxide ligand. The exact value of ν(Fe-OH) can, however, not be determined without isotope labelling experiments due to the expected overlap with other modes in this region [17].

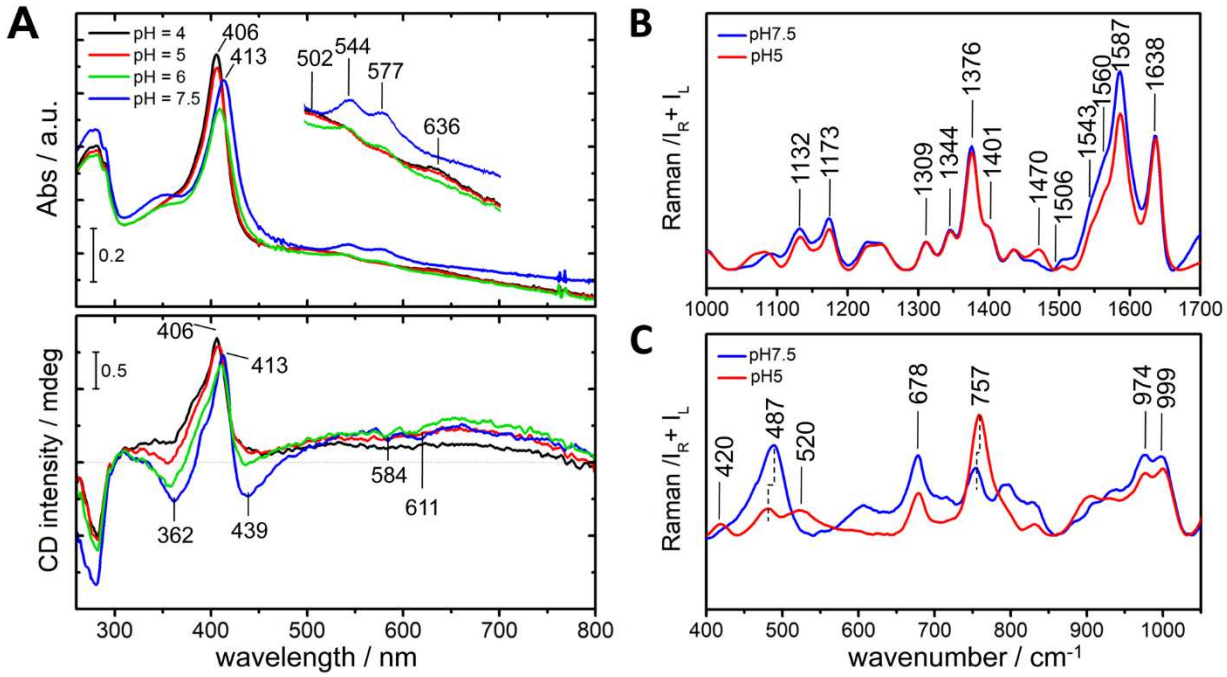

Figure 1. (A) UV/Vis Abs (top) and ECD (bottom) spectra of 25 μM ferric GLB-33GDΔCys in sodium acetate (pH 4.0, 5.0) or Tris-HCl buffer (pH 6.2, 7.5). Inset: The Q-band area of the spectrum is shown magnified for facile comparison. B and C: high and mid frequency rRaman spectral regions, respectively, of 25 μM ferric GLB-33GDΔCys at pH 5.0 and 7.5.

At pH 5.0, the rRaman spectral signature changes completely in this wavenumber region with two signals now observed around 485 cm^{-1} and 520 cm^{-1} (Fig. 1C). While ν(Fe-OH) ≈ 490 cm^{-1} is

typically reported for 6c/HS species in an aquomet form [51], the observation of a peak at 520 cm^{-1} may point to the presence of residual 6c/LS form with weaker hydrogen bonding stabilization [49]. This interpretation should, however, be considered with caution, because no isotope labelling was performed.

CW-EPR spectra of ferric hydroxo-ligated globins are known to be strongly influenced by the degree of hydrogen bonding to the hydroxide ligand. Figure 2A shows the experimental and simulated X-band CW-EPR spectra of GLB-33GDΔCys at different pH. At neutral pH, the spectrum is dominated by the contribution of two 6c/LS forms, with a negligible fraction of a HS haem (Table 1). The two 6c/LS forms, indicated by LS1 and LS2, agree with what was observed earlier at pH 8.5 for GLB33GD [16]. The assignment of the different spectral components to LS1 and LS2 is confirmed by temperature-dependent EPR (Figure S3, supplementary material).

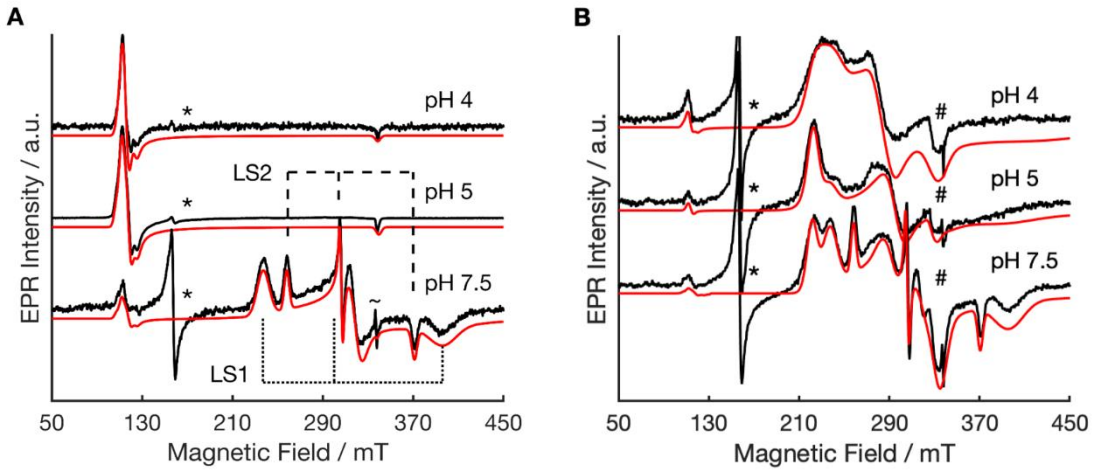

Figure 2. Experimental and simulated X-band CW-EPR spectra of frozen solutions of ~1 mM ferric GLB-33GDΔCys in the absence (A) or presence (B) of 50x molar excess nitrite at pH 4.0, 5.0 and 7.5. Nitrite-treated samples (B) were immediately frozen after mixing to minimize the formation of green pigment (nitri-globin formation). The spectra were recorded at 10 K with a microwave power of 100 mW. Organic radical (#), background signal due to Cu(II) traces in the sample (~) and non-haem iron (*).

Table 1. Principal *g* values and zero-field parameters (*E/D*) of the low-spin (*S*=1/2) and high-spin (*S*=5/2) species of ferric GLB-33GDΔCys obtained through simulation of the spectra in Figure 2A in comparison with literature data. Simulations of the individual components contributing to the spectra in Figure 2A are shown in Figure S4. n.a. = not applicable; n.d. = not determined; Mb = myoglobin; *Al*Mb= *Aplysia limacina* Mb; *Lp*Hb II = Hb II from *Lucina pectinate*; *Tf*-TrHb = truncated Hb 1 from *Thermobifida fusca*; *Cr*TrHb1 = truncated Hb 1 from *Chlamydomonas reinhardtii*. Experimental errors on principal *g*-values of LS species (±0.01) and HS species (±0.003), on *E/D* (±0.005) and % (2). For the simulation of the HS species, *D* was taken to be equal to 10 cm^{-1}.

System	**Label**	g_x	g_y	g_z	***E/D***	**%**	**coordination**	**Ref**
GLB-33GDΔCys pH 7.5	LS1	1.70	2.22	2.84	n.a.	75	His/OH^-	This work
	LS2	1.82	2.20	2.61	n.a.	23	His/OH^-	
	HS1	1.957	1.957	1.984	0.0069	1	His/H_2O	
	HS2	1.958	1.958	1.999	0.0180	1	His/H_2O?	
GLB-33GD pH 5.0	LS1	1.70	2.22	2.84	n.a.	9	His/OH^-	This work
	LS2	1.82	2.20	2.61	n.a.	2	His/OH^-	
	HS1	1.957	1.957	1.984	0.0069	67	His/H_2O	
	HS2	1.958	1.958	1.999	0.0180	33	His/H_2O?	
GLB-33GDΔCys pH 4.0	HS1	1.968	1.968	1.991	0.0045	65	His/H_2O?	This work
	HS2	1.950	1.950	1.999	0.0159	35	His/H_2O	
Mb pH=7.5	n.a.	1.98	1.98	2.00	0.0025	n.d.	His/H_2O	[53]
Mb alkaline	n.a.	1.85	2.17	2.55	n.a.	n.d.	His/OH^-	[54]
*Al*Mb pH 10.0	n.a.	1.75	2.10	2.72	n.a.	n.d.	His/OH^-	[55]
*Lp*HbII alkaline	n.a.	1.82	2.20	2.61	n.a.	n.d.	His/OH^-	[54]
Tf-TrHb pH 6.0	n.a.	1.60	2.32	2.82	n.a.	n.d.	His/OH^-	[17]
	n.a.	1.76	2.19	2.73	n.a.	n.d.	His/OH^-	
	n.a.	1.81	2.19	2.66	n.a.	n.d.	His/OH^-	
Cr-TrHb1 K53R	n.a.	1.66	2.21	2.78	n.a.	n.d.	His/OH^-	[56]

LS2 has principal *g* values that agree with what has been reported before for the hydroxo-form of Mb and related globins and are indicative of minor to no hydrogen bonding of the hydroxide [54]. In contrast, the dominant LS1 species is more similar to the hydroxo-ligated species found in the truncated haemoglobins and their variants in which strong hydrogen bonding networks keep the hydroxide in place (Table 1, [17,56]). This corroborates the above tentative conclusions drawn on the basis of the rRaman spectra (Figure 1C). The CW-EPR spectrum of GLB-33GDΔCys at pH 5.0 shows a minor LS fraction next to a large signal due to HS haem species, whereas at pH 4.0,

only the contribution of the HS centres remains. The *E/D* values of the HS forms (Table 1) are characteristic for 6c/HS [53] and thus confirm the room-temperature rRaman and UV/Vis Abs data. The slight variations in the EPR data of the HS forms may result from pH-dependent small changes in the dielectric constant and/or small variations in the orientation of the axial water ligand in the haem pocket. The relatively small *E/D*-values of some of the 6c/HS forms are in line with what has been observed for aquomet globins.

3.2 Effect of addition of nitrite to ferric GLB-33GDΔCys at different pH values

In a second step, the effect of addition of a 50-fold excess of sodium nitrite to ferric GLB-33GDΔCys is studied at different pH values. Only a small reduction in the high wavelength flank of the Q_α band of the UV/Vis Abs spectrum of ferric GLB-33GDΔCys is observed with increasing nitrite concentration at pH 7.5 (Supplementary information, Figure S5). The respective ECD spectrum shows no significant changes compared to the untreated sample at pH 7.5 (Figure 3C). In contrast, the nitrite treatment at pH 4.0 and 5.0 leads to substantial changes in the UV-Vis Abs/ECD spectra of GLB-33GDΔCys (Figures 3A and B). An initial redshift of the Soret band from 406 nm to 416 nm and $Q_{\beta,\alpha}$ bands at 564 nm and 544 nm was observed in agreement with the reported spectra of nitrite-ligated cytochrome c' [57]. They indicate a shift from a 6c/HS to a 6c/LS state. These Abs spectra are considerably different from those observed for ferric Mb after addition of NO_2^- near neutral pH [58]. The ECD spectra of GLB-33GDΔCys with nitrite at acidic pH exhibit reduced, red-shifted Soret ellipticity, with a sharp, negative dichroic band and a broader, negative, and less pronounced ECD band appearing at 426 nm and 570 nm, respectively (Figure 3A, B).

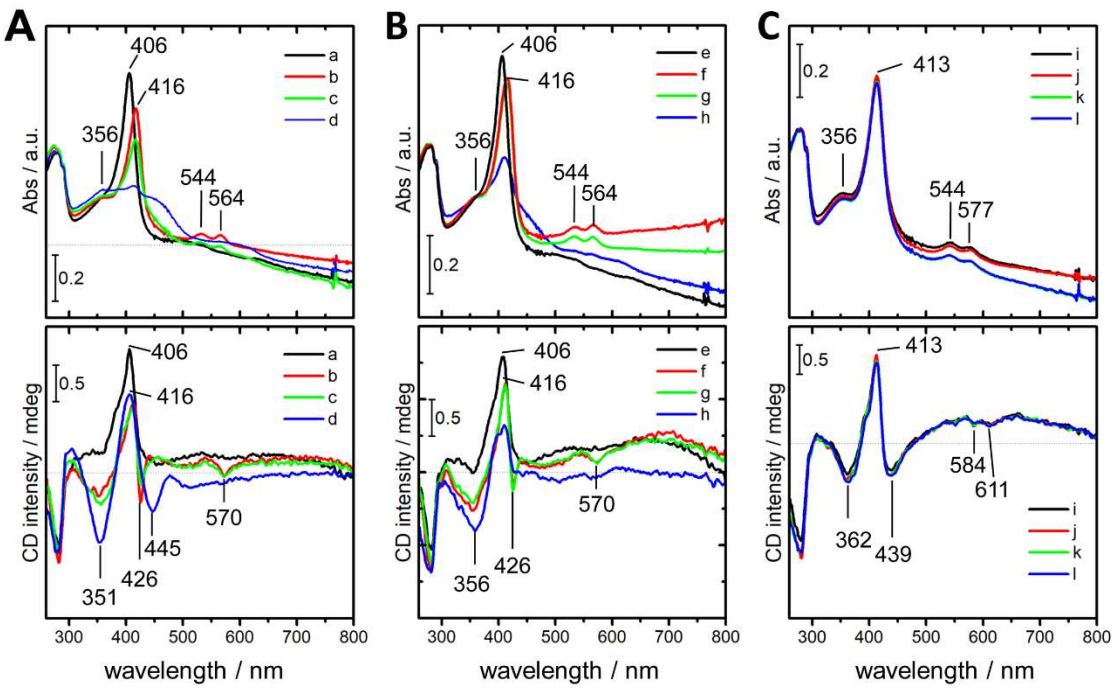

Figure 3. UV/Vis Abs (top) and ECD (bottom) spectra of 0.025 mM GLB-33GDΔCys before (a, e, i) and after addition of 1.2 mM $NaNO_2$ at $t = 0$ (b, f, j), at $t = 240$ min (c, g, k), and at $t = 24$ hrs. (d, h, l). The spectra were collected at pH 4.0, 5.0 and 7.5 (Panel A, B and C, resp.).

Figure 3 also shows the effect of incubation time with nitrite on the UV/Vis Abs and ECD spectra of ferric GLB-33GDΔCys at pH 7.5, 5.0 and 4.0. At pH 4.0 and 5.0 the formation of a green pigment could be observed visually, in line with the strong spectral modifications in the Abs/ECD spectra (Figure 3A, B). Long (24h) incubation times at pH 4.0 and 5.0 with nitrite lead to a reduction in the Soret Abs band, a broadening of the B band, and the appearance of a maximum at 356 nm. Green pigment formation with these associated Abs spectra point to the formation of a vinyl-nitrated globin derivative (nitri-globin) [59]. In the corresponding ECD spectra of nitrite-incubated GLB-33GDΔCys, the Soret ellipticity broadens over time with a concomitant broadening of the band at 426 nm, which shifts up to 448 nm. Finally, the negative ellipticity centred around 351-356 nm becomes dominant, with a corresponding disappearance of the negative ellipticity at 570 nm. ECD spectroscopy in the far UV-region demonstrates that the secondary structure composition is largely retained at the experimental conditions used for our purpose (Figure S2).

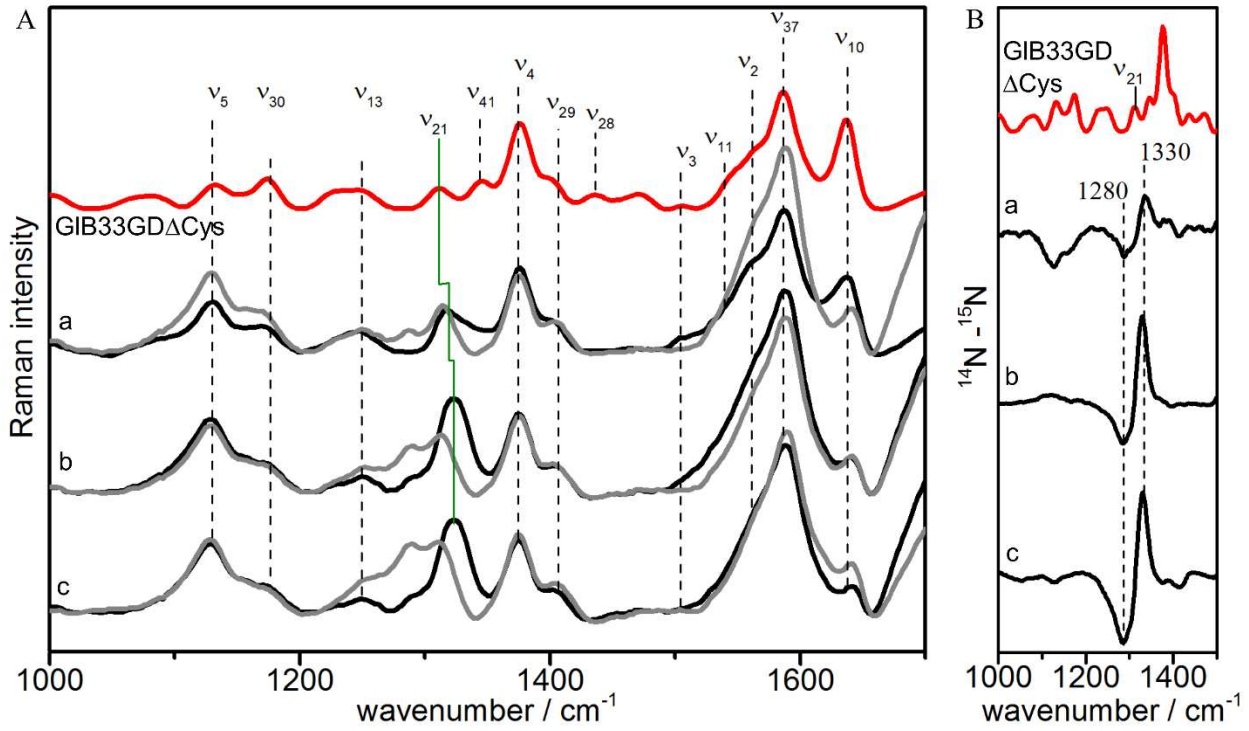

Figure 4. Panel A: rRaman spectrum of GLB-33GDΔCys (red) treated with (a) 50, (b) 280 and (c) 500 molar excess of $^{14}NO_2^-$ (black) and $^{15}NO_2^-$ (grey) in acetate buffer at pH 5.0. In green the rRaman shift of the mode ν_{21} is marked. Panel B: high frequency difference rRaman spectra of GLB33GDΔCys-$^{14}NO_2^-$ minus GLB33GDΔCys-$^{15}NO_2^-$.

The rRaman spectra of the nitrite-treated ferric GLB-33GDΔCys at various pH-values follow the observations with UV/Vis Abs spectroscopy (Figure 4, Figure S6). At pH 7.5, the spectrum did not reveal changes in the spin and/or ligation state of the haem iron with respect to ferric GLB-33GDΔCys (Figure S6). At pH 4.0 and 5.0 in contrast, a strong reduction in the ν_{10} Raman intensity and changes in the relative ratio between the Raman bands ν_{37} and ν_{10}, and between ν_5 and ν_{30} are observed (Figure 4, S6).

In the presence of nitrite, the vinyl stretching mode ν_{21} is found to be pH dependent (Figure S6). Figure 4 highlights the nitrite-concentration dependence and isotopic dependence of this mode at pH 5.0. This dependence agrees with nitrovinyl formation in line with the visually observed formation of a green pigment (nitri-globin formation, see Figure S1C,F for schematic representation and example of nitrivinyl formation).

Table 2. Principal *g* values of the 6c/LS species observed in the EPR spectra of ferric GLB-33GDΔCys after addition of sodium nitrite at different pH values. Small contributions (~1%) of residual 6c/HS species were observed. Numbers as obtained through simulation of the spectra in Figure 2B. The parameters are shown in comparison with literature data for other NO_2^--bound globins. n.a.= not applicable; n.d. = not determined; (sw)Mb=(sperm whale) myoglobin; Hb=vertebrate haemoglobin; NP=nitrophorin; Cyt c'= cytochrome c', Cld = chlorite dismutase. Experimental errors on $g_{x,y}$: ±0.03 at pH 7.5 and 5, ±0.05 at pH 4.0, g_z: ±0.01 at pH 7.5 and 5, ±0.03 at pH 4.0, and on %: 2.

System	Label	g_x	g_y	g_z	%	coordination	Ref
GLB-33GDΔCys pH 7.5	LS1	1.70	2.12	2.84	41	His/OH^-	This work
	LS2	1.82	2.20	2.61	8	His/OH^-	
	LS3	~1.53	2.29	3.03	51	His/NO_2^-	
GLB-33GDΔCys pH 5.0	LS3	1.53	2.26	3.00	93	His/NO_2^-	This work
	LS1*	1.70	2.07	2.84	7	His/OH^-	
GLB-33GDΔCys pH 4.0	LS3*	1.53	2.13	3.01	46	His/NO_2^-	This work
	LS4	~1.38	2.35	2.84	54	His/NO_2^-	
Mb pH 7.0	n.a.	1.57	2.20	2.95	100	His/NO_2^-	[32]
H64V (sw)Mb pH 7.0	n.a.	n.d.	~2.1-2.3	3.16	89	His/NO_2^-	[60]
	n.a.	n.d.	~2.1-2.3	2.93	10	His/NO_2^-	
Hb pH 5.0-10.0[a)]	LSA	1.45	2.30	2.87	(a)	His/NO_2^-	[61]
	LSB	1.45	2.12	3.02	(a)	His/NO_2^-	
NP7 pH 7.2	n.a.	1.46	2.34	2.86	n.d.	His/NO_2^-	[62]
	n.a.	1.46	2.40	2.78	n.d.	His/NO_2^-	
NP4 pH 7.2	n.a.	1.51	2.42	2.74	n.d.	His/NO_2^-	[62]
	n.a.	n.d.	n.d.	3.38	n.d.	His/NO_2^-	
Cyt c' pH 7.0	n.a.	1.56	2.36	2.84	n.d.	His/NO_2^-	[57]
	n.a.	n.d.	2.2	3.25	n.d.	His/NO_2^-	
Cld pH 7.0	n.a.	1.55	2.18	2.93	n.d.	His/NO_2^-	[63]

(a) relative intensity varies with pH [61]
(*) similar to LS1/LS3

While the optical methods used above (Figures 3 and 4) clearly indicate nitration of the haem vinyl groups, they are less informative on the haem-iron ligation. At pH 7.5, little to no changes are observed in the UV/Vis Abs, ECD and rRaman spectra of ferric GLB-33GDΔCys upon addition of nitrite. Nevertheless, an additional component due to a 6c/LS species is observed in the corresponding EPR spectrum (Figure 2B, see Figure S7 for assignment of peaks). This component (LS3) has EPR parameters that are similar to the ones observed for nitrite-ligated myoglobin

(Table 2). The lower g_x value is hard to determine, but it can be estimated using electron-spin-echo (ESE)-detected EPR at X-band (Figure S8). Note that at pH 7.5, only partial replacement of the hydroxide ligand by nitrite is observed for ferric GLB-33DΔCys. A previous study of nitrite binding to human haemoglobin revealed a replacement of the nitrite ligand by hydroxide at high pH [61], indicative of a stronger affinity of the haem center to hydroxide than to nitrite. The contribution of a HS ferric haem form remains negligible (<1%). As evidenced by the rRaman spectra, nitrite-binding at this pH does not trigger a further nitration of the haem vinyl groups.

At pH 4.0 and 5.0, a strong change in the EPR spectra of nitrate-ligated GLB-33GDΔCys is observed. The HS contributions almost completely disappear (<1%) and new signals due to two 6c/LS species appear (LS3 and LS4, Table 2, Figure 2B, see Figure S7 for assignment of peaks). The shift in the spin state indicates that next to nitration of the vinyl, also nitrite-ligation to the ferric haem iron occurs. Again, the g_x value for the low-pH 6c/LS species of GLB-33GDΔCys is not detectable in the CW-EPR spectra due to the large *g*-strain, but from ESE-detected EPR experiments an upper limit for the g_x value can be estimated (Figure S9). At pH 5.0, LS3 is dominating the spectrum, while at pH 4.0, the dominant contribution shifts to LS4. Small pH dependent shifts of the g_z value are observed for the EPR parameters of LS3. Similar small shifts have been observed for the EPR parameters of LSB in nitrite-ligated human haemoglobin (Table 2, [61]).

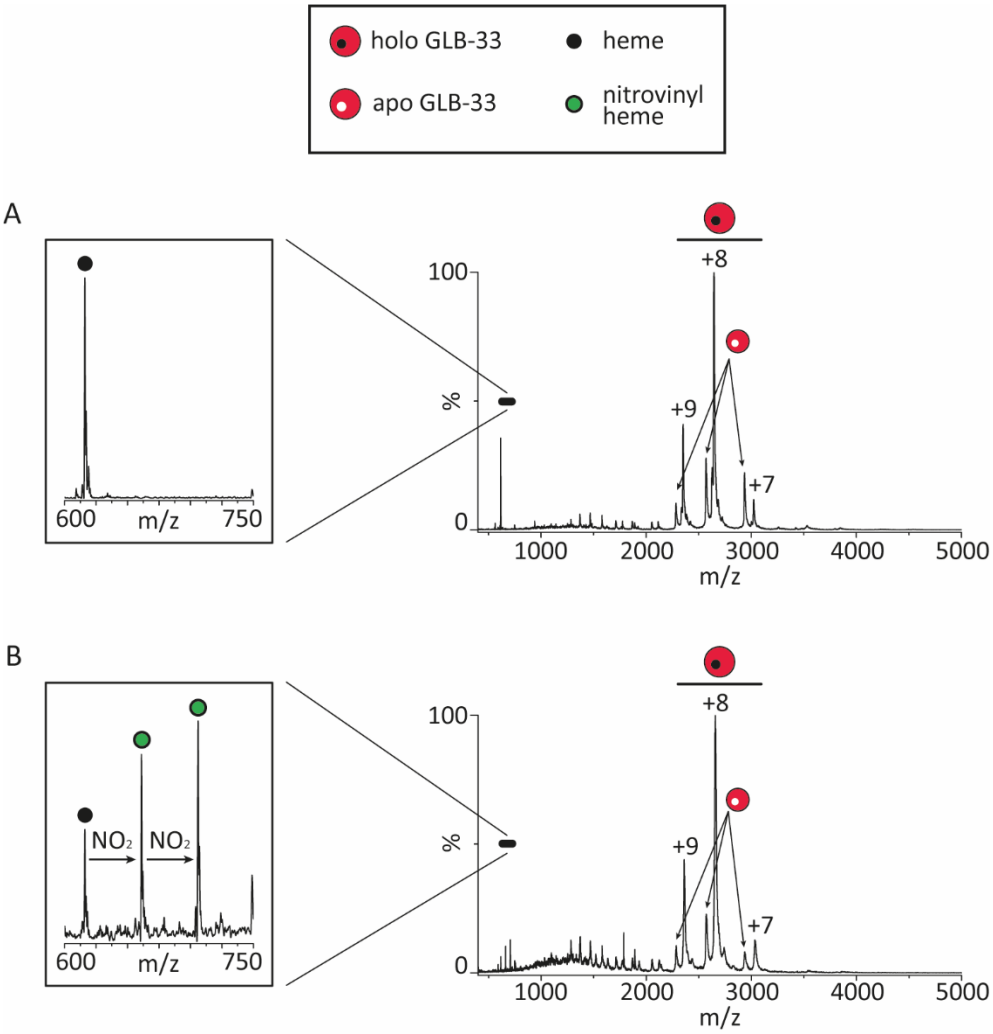

Figure 5. Native MS spectra of GLB-33GDΔCys after incubation with 50-fold excess of sodium nitrite at pH 7.5 (A) and 4.0 (B). The narrow charge state distribution (+7 to +9) corresponds to monomeric holo GLB-33GDΔCys. Satellite peaks indicate a minor fraction of the apo-form. The inset shows the m/z area between 600 and 750, which highlights that nitrite binding only occurs at pH 4.0.

To corroborate the spectroscopic findings on the pH-dependent effect of nitrite addition to ferric GLB-33GDΔCys, we performed native mass spectrometry (MS) measurements after incubation with 50-fold molar excess of sodium nitrite at pH 4.0 and 7.5 for 24 hours. Native MS describes a method in which analytes are transferred from solution to the gas phase while aiming to maintain the solution-phase structure through careful control of crucial parameters [64-70]. Hence, in case of GLB-33GDΔCys, we can retrieve information of whether the treatment with sodium nitrite leads to covalent nitrate-ligation of the haem group.

The spectra show for both samples, *i.e.* sodium nitrite treatment at pH 4.0 and 7.5, a narrow charge state distribution of monomeric GLB-33GDΔCys, indicating the native, folded character of the holo protein (Figure 5). Only a minor population of the protein is unfolded – evidenced by the presence of higher charged complexes at around 1000-2000 m/z – and/or lacks the haem group (apo form). Such minimal protein unfolding was also observed in the negative control (no nitrite addition) of GLB-33GDΔCys (Figure S10), indicating that unfolding occurred due to non-optimal solution conditions, or the protein being kept at room temperature for 24 hours rather than by the sodium nitrite treatment. The inset highlights the range between 600 and 750 m/z, the area where (nitrovinyl) haem would be expected. Nitrovinyl haem – covalent modification of the vinyl groups with one and even two nitrite molecules (Figure S1C,F) – is only present after sodium nitrite treatment at pH 4.0, confirming previous spectroscopic findings that the pH is crucial for the binding of nitrite. The formation of nitrovinyl haem is indicated by an increase of 44.98 m/z (haem: 616.13 m/z; nitrovinyl haem: 661.11 m/z; charge state: +1), implying the replacement of an H-atom for each nitrite molecule bound.

3.3 Nitro or nitrito binding to the haem iron?

Both species LS3 and LS4 seem to be due to a nitrite-ligated haem species, albeit with a different pH dependence (Table 2). The observation of multiple LS species in the EPR spectra of ferric haem proteins after addition of nitrite is not uncommon [32,57,60-62]. The variation in the EPR spectra has been ascribed to multiple effects, such as hydrogen-bonding effects, haem ruffling or nitro- versus nitrito ligation [32,71]. The principal *g* values can be linked to crystal-field parameters by a simple calculation [72]. In the supplementary material (Table S1, Figure S11), the crystal-field parameters of LS3 and LS4 and other nitrite complexes of haem proteins are calculated and plotted in a "Blumberg-Peisach" diagram. LS3 and LS4 fall in different regions of the diagram. In a recent work on the nitrite complexes of chlorite dismutases by some of us [32], a link was made between the area in this diagram in which the crystal-field parameters fall and the nitrite-binding mode (N-nitro versus O-nitrito), corroborated by XRD and molecular modelling. Following this reasoning, the nitrite complex observed at pH 7.5 (LS3) is tentatively ascribed to the nitrito-complex, while lowering of the pH induces the nitro binding mode (LS4).

In order to substantiate this assumption, pulsed EPR experiments were performed. At pH 7.5, the presence of the EPR contribution of the hydroxide complexes of GLB-33DΔCys (LS1 and LS2)

complicate the analysis of the nitrite-ligated species. Only the magnetic-field position agreeing with $g=g_z$ of species LS3 can be attributed solely to the nitrite-ligated GLB-33DΔCys. Figure 6A shows the two-pulse ESEEM time trace taken at this position for a frozen solution of GLB-33DΔCys in the presence of $Na^{14}NO_2$ (red) and $Na^{15}NO_2$ (blue). Small changes due to the isotope change are observed in the modulation pattern. By dividing the two traces (Figure 6A, inset) and subsequent Fourier transformation (Figure 6B), a clear peak at 7.4 MHz is observed, with smaller signals at lower frequency. The three-pulse ESEEM experiment performed at the same observer position also showed small changes in the low frequency range (Figure S12). In the corresponding HYSCORE spectra, the differences were less clear (Figure S13), however, for this experiment, the observer position had to be set slightly more up field in order to still have a significant echo signal. At this observer position, contributions of LS1 will start to contribute, potentially masking the small isotope-labelling-induced differences in the LS3 contribution. The clearest isotope-induced changes are seen in the two-pulse ESEEM experiment, but the assignment of the peaks remain unclear, but indicate ^{14}N hyperfine couplings <7 MHz (in absolute value).

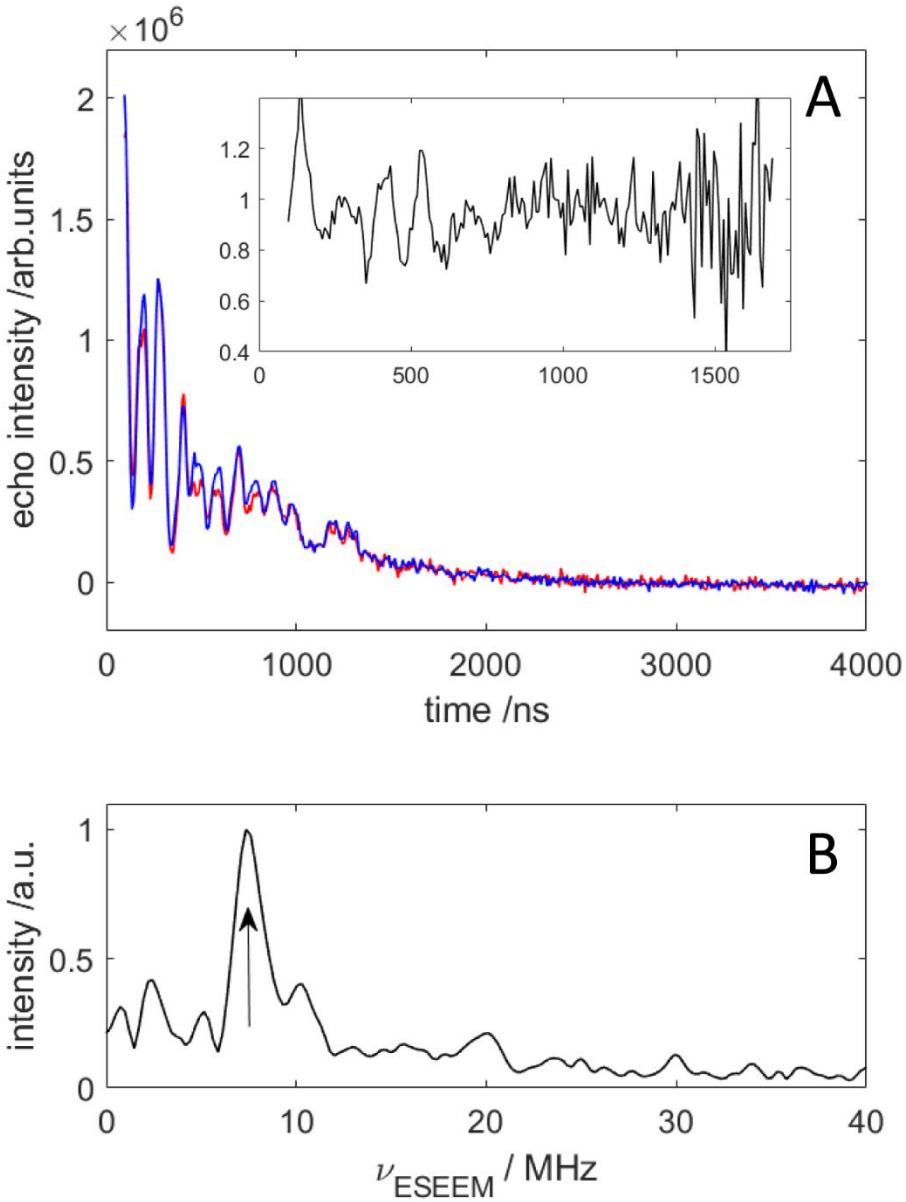

Figure 6. (A) Comparison between the two-pulse ESEEM time traces of frozen solutions of ~ 1 mM ferric GLB-33GDΔCys at pH 7.5 after addition of a 50-fold excess of $Na^{14}NO_2$ (red) and $Na^{15}NO_2$ (blue). 25 % (v/v) glycerol was added to the solution as a cryoprotectant. The spectra were recorded at 235 mT, an observer position agreeing with $g = g_z$ of LS3. The inset shows the division of the two time traces. Only the first half of the trace is shown, since for signals near zero intensity, the noise increasingly contributes. (B) Fourier transform of the time-domain signal in the inset.

3.4 Nitrosylated GLB-33D

Ferrous GLB-33GD can act as a nitrite reductase, leading to an NO-bound GLB-33GD (Fe^{2+}-NO) form with Q-band absorption bands at 545 and 570 nm [16]. This ligation state is here confirmed by low-temperature X-band EPR spectrum of ferric GLB-33GD reduced using dithionite and subsequently treated with nitrite (Figure 7), revealing the typical EPR characteristics of a His - Fe^{2+} - NO coordination also found other globins [73-76]. The EPR spectrum consists of two components, characterized by an axial and a rhombic ***g*** tensor, respectively (Figure 7), in line with the presence of at least two conformational states of the distal NO ligand in line with findings for other nitrosylated globins [73-76]. The rhombic form also shows additional splitting due to the hyperfine interactions with the ^{14}N nucleus of the distal NO ligand and of the Fe-bound nitrogen of the proximal His, with the hyperfine values being $[A_1\ A_2\ A_3]$ = [32 62 39] ± 3 MHz for ^{14}N(NO) and $[A_1\ A_2\ A_3]$ = [25 20 30] ± 2 MHz for ^{14}N(His).

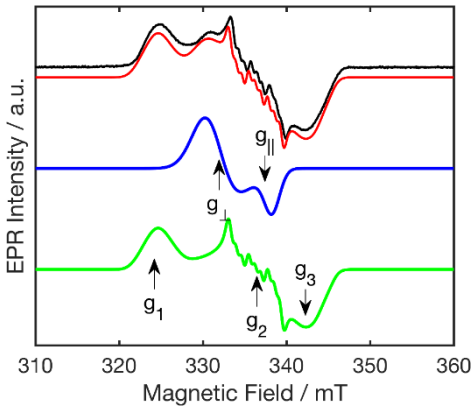

Figure 7 Experimental (black) and simulated (red) EPR spectrum of a frozen nitrosylated GLB-33GD solution recorded at 2.6 K. The simulated spectrum is built up by a component with an axial ***g*** tensor (blue, $g_\perp$= 2.0361 and $g_\parallel$ = 1.9946) and one with a rhombic ***g*** tensor (green, g_1 = 2.0776, g_2 = 2.0047 and g_3 = 1.9682). Magnetic field positions corresponding to the g values are indicated by the arrows. The ^{14}N hyperfine couplings are mentioned in the text.

4. Discussion

Caenorhabditis elegans is a promising model for globin studies as it encodes 34 globins out of which only a handful have been characterized biochemically *in vitro*. GLB-33 is the largest of its kind, chimeric, consisting of an FMRF-amide binding and membrane binding domain, and a globin domain. An initial biochemical characterization by some of us [16] revealed both an unusual hydroxo ligation of the ferric state at slight acidic pH and a fast nitrite reductase activity. Here we show that the nitrite reductase reaction leads to formation of a nitrosylated ferrous form in which the haem is still bound to the proximal histidine. NO ligation is known to weaken the Fe-N(His) bond and leads in some globins and other haem proteins to the breaking of this bond [77,78]. Earlier work using combined high-field EPR and quantum-chemical computations, ascribed the observation of the two forms in the EPR spectrum of nitrosylated myoglobin to changes in the stabilization of the NO ligand via H-bonding with the E7His residue, with strong H-bonding inducing the species with rhombic ***g*** tensor, and a weaker interaction leading to the species with axial ***g*** tensor [79]. GLB-33GD has, however, no His on the E7 position and has a highly hydrophobic haem pocket [16]. Furthermore, earlier work on a variant of neuroglobin in which the E7 residue was mutated to Leu also showed the presence of the two nitrosylated ferrous forms [75], indicating that the formation of the two forms is governed by more than the capacity of the E7 ligand to form H-bonds.

The EPR spectrum of ferric GLB-33GDΔCys at pH 4.0-5.0 is typical for a HS ferric form with a weak distal ligand in line with the presence of an aquomet form. However, at pH 7.5 an alkaline transition to two hydroxo-ligated forms has happened, of which one form (LS1) has EPR parameters similar to those observed in globins [17] in which the hydroxide is stabilized in a strong hydrogen-bonding network. In haem proteins, the pK_a of the alkaline transition (distal water to hydroxo ligand) is known to be determined by many factors, including the presence of distal hydrogen-bonding networks [17], distal salt bridges [80] and the proximal ligand [60]. In contrast to ferric sperm whale Mb (swMb) that exhibits an alkaline transition at pK_a 8.9 [60], the pK_a of the alkaline transition in myoglobin from *Aplysia limacina* (*Al*Mb) is found to occur at lower pH (pK_a 7.5) [81]. The latter myoglobin resembles GLB-33GD(ΔCys) with hydrophobic residues on positions E7 (Val) and E11 (Ile). Both *Al*Mb and GLB-33GD(ΔCys) have an Arg on position E10.

In *Al*Mb, the Arg at position E10 is found to be able to swing into the distal haem region and stabilize anionic ligands bound to the haem iron (Figure S15), an effect that can be also induced in swMb variants carrying the His(E7) to Val mutation [82,83]. A similar process seems to occur here, where LS1 then points to a form in which the hydroxo ligand is stabilized by Arg(E10) and LS2 is a less stabilized form, potentially related to a movement of the Arg residue. This is further supported by the strong resemblance between the *g* values of LS1 and the LS component found at pH 10.0 for *Al*Mb (Table 1, [55]). Interestingly, the haem iron in ferric *Al*Mb is five-coordinated below the alkaline transition (Figure S15A, [84]). This seems to be in contrast with GLB-33GD(ΔCys), for which the EPR spectrum at low pH is typical for axial ligation of a weak ligand, most likely water.

A comparable pH effect has also been observed for chlorite dismutase from *Cyanothece* sp. PCC7425 (*C*Cld) [80]. In this haem-*b* containing peroxidase that can decompose chlorite, a distal arginine (Arg127) is known to play a crucial role in enzyme activity. Arg127 can switch between two conformations in and out of the distal region, whereby the outward conformation is hydrogen-bonded to glutamine 74. The alkaline transition occurs in wild-type ferric *C*Cld at pK_a 8.11 and EPR reveals the presence of 3 LS forms at high pH, with the principal *g*-values agreeing with varying degrees of H-bonding, comparable to what is observed for GLB-33GDΔCys. When Arg127 is halted in the outward position through a salt bridge to glutamic acid in the Q74E *C*Cld variant, the pK_a shifts upwards (9.33), while a mutation of Gln74 to Val, thus allowing more flexibility of Arg127, leads to a considerable down-shift of the pK_a (7.41). This also has a large impact on the relative ratio of the three LS forms in the EPR spectra with the form that points to the strongest H-bonding with Arg127 becoming more prevalent in the Q74V variant and almost disappearing in the Q74E variant, where the Arg127 is locked in the outward position.

The pH-dependent ECD spectra of GLB-33GDΔCys in the near UV to visible range differ from those of horse heart myoglobin (hhMb) (Figure S14). The ECD spectra of hhMb are showing a much higher magnitude of the Soret ellipticity and less negative contribution in the *N* region (300-350 nm) compared to GLB-33GD at neutral to alkaline pH. This shows that the substitution of hydroxide ligand is not a major contributor to the observed negative ellipticity for GLB-33GD, but that rather the differences in haem pocket structure are determining the spectral fingerprint. This is corroborated by the comparison with the pH-dependent ECD spectra of *C*Cld and its Q74

variants [80], where the alkaline transition reduces the negative ellipticity in contrast to what is observed here. Although the ECD spectra are highly dependent on amino acids surrounding the haem, the planarity of the haem itself, and the haem insertion [44-47], there is still a lack of thorough (theoretical) understanding that hampers a facile linking of these data to specific features of the haem pocket. This can potentially be circumvented by using MCD (magnetically circular dichroism) in future studies [85], as demonstrated for nitrite ligation to Mb [60].

Addition of nitrite to ferric GLB-33GDΔCys leads at neutral pH to a competition of nitrite with the hydroxo ligands, with a co-existence of both hydroxo (LS1,2) and nitrite-ligated (LS3) species observed with EPR (Table 2). Comparison of Table 1 and Table 2 reveals that the hydroxo ligand of LS2 gets more easily replaced by nitrite than is the case for LS1. This is in line with the stronger hydrogen bonding to the Arg ligand in the latter complex. The principal *g* values of LS3 are typical for nitrite-ligated haem proteins exhibiting a nitrito bonding mode (Fe-O bond) (Table 2, Figure S11) and this assignment is corroborated by the ESEEM analysis showing signals that agree with ^{14}N hyperfine values (in absolute value) well below 7 MHz. A quantumchemical study on the linkage isomers of nitrite-ligated Mb predicts small ^{14}N hyperfine coupling parameters for the nitrito form, while a nitro form would lead to hyperfine values around 20 MHz (in absolute value) [87]. At pH 5.0, LS3 has become the dominant species, while at pH 4.0, the EPR spectrum broadens and a second LS complex is found (LS4) to co-exist with an LS3-like species. Moreover, the UV/Vis Abs and ECD spectra show that acidic pH leads to formation of a vinyl-nitrated haem (nitri-globin), an effect that is more pronounced at the lowest pH and is also observed for other haem proteins [29]. The principal *g*-values of LS4 seem to be more consistent with a nitro-form (Fe-N bond) (Table 2, Figure S11).

X-ray crystallography of nitrite complexes of ferric hhMb and variants revealed an interesting interplay between the E7 and E10 ligand in directing the nitrite binding mode [43]. While ferric nitrite-ligated Mb shows a nitrito form with the nitrite ligand H-bonded to E7His (Figure S1E), mutation of the E7His to Val (H64V) in Mb leads to a weakly bound nitro form (Figure S1D). Interestingly, the nitrito form is recovered in the double mutant carrying also the E10Val-to-Arg mutation (H64V/V67R) in which Arg now acts as the H-bonding residue (Figure 8B). This is accompanied by a swinging of the Arg into the haem pocket (Figure 8, [43]). A similar effect is proposed to happen in GLB-33GD(ΔCys). Also in nitrite-ligated ferric *C*Cld the distal Arg residue

stabilizes the nitrito form [32]. ArgE10 is therefore crucial in stabilizing the LS3 nitrito form of ferric GLB-33GDΔCys. Formation of the nitro form (LS4) at pH 4.0 may potentially be due to the nitriglobin formation and, even some onset of protein denaturation upon freezing of the solution. Although the latter can never be excluded at any pH, it is more likely to occur at pH 4.0, because freezing can lower the pH even further.[86] This will alter the haem pocket and can influence the conformation and orientation of the E10Arg residue. If no H-bonding residue is nearby, the nitro form will be formed, in line with the observation for H64V hhMb (Figure S1D [43]).

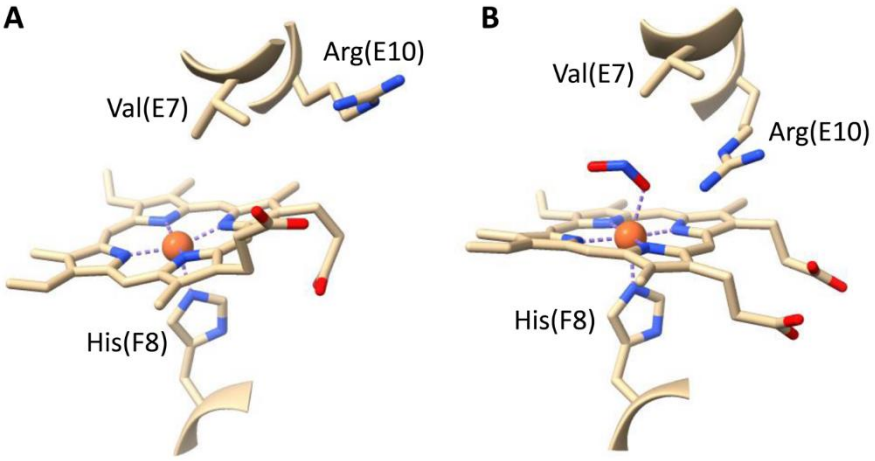

Figure 8. Structural change observed in the haem pocket of H64V/V67R variant of hhMb upon binding of nitrite. Val64 is at position E7, Arg67 is at position E10. (A) Structure with no distal ligand present (PDB ID: 3HEN). (B) Structure with nitrite in nitrito form (PDB ID: 3HEO). The figure illustrates the swinging of the Arg residue in (B) and out (A) of the haem pocket. A similar effect is proposed here for GLB-33GD(ΔCys).

The ECD spectra of ferric GLB-33GDΔCys with nitrite at pH 4.0 and 5.0 (Fig. 3 A, B) showed a strong evolution over time in at least three of the four main regions where the plane polarized transitions were detected (*Q*: 470 - 600 nm; *B*: 380 - 450 nm; *N*: 300-350 nm; *L*: 250-320 nm). While absorption and ECD spectra in the aromatic region remained unchanged upon the treatment of the globin with NO_2^-, a gradual increment of the overall ellipticity with a minimum at 351 and 356 nm for pH 4.0 and 5.0, respectively, was observed. A large enhancement of the *N* dichroic band (300-400 nm) has been described in literature for the model system of *Lucina pectinata* Hb (*Lp*Hb) as the result of a resonant interaction between the electronic transition of the aromatic residues and those of the *N* and *L* bands, because of their simultaneous excitation [88]. However, this effect is less likely to happen in GLB-33GDΔCys, since the amount of aromatic residues near

the haem is much lower than in *Lp*Hb. Noteworthy, at pH 4.0 and 5.0, the *B* dichroic band at 416 nm is in first instance slightly reduced in magnitude (during the first 8 hours), and at the same time the two negative dichroic bands appear. In particular, the sharp negative ECD band at 426 nm and the broader negative ellipticity at 570 nm are prominent after addition of nitrite. Potentially, these signals are markers for the nitrite ligation. Finally, acidified solutions of NO_2^- contain NO (disproportionation reaction). Therefore, besides an Fe(III)- NO_2^- complex, a fraction of Fe(III)-NO could in principle be formed [89]. EPR spectroscopy is not suited to detect this form as it is EPR silent ($S = 0$), but UV-vis Abs spectroscopy is not showing any evidence that such species and formation of a nitrosylated ferric form is therefore excluded.

The nitrite reductase activity of GLB-33GD has been modelled with a fast second order rate constant k_{NIR} of 36.3 $M^{-1}s^{-1}$ [16]. This is high in comparison with other globins (e.g. for hhMb k_{NIR} values of 5.5 $M^{-1}s^{-1}$ [43] to 6.1 $M^{-1}s^{-1}$ [90] are reported). Interestingly, the H64V hhMb mutant has a strongly reduced nitrite reductase activity (k_{NIR} = 0.35 $M^{-1}s^{-1}$), while this is partially restored in the H64V/V67R double mutant (k_{NIR} = 1.8 $M^{-1}s^{-1}$) [43]. This illustrates again the important effect of E10Arg when no H-donating residue is present on position E7, in line with our findings for binding of hydroxide or nitrite. However, the presence of the E10Arg is clearly not enough to explain the enhanced nitrite reductase activity of GLB-33GD. While the H64A hhMb variant shows a strong reduction of the nitrite reductase activity (k_{NIR} = 0.1 $M^{-1}s^{-1}$), a remarkable increase of this activity is reported for the F43H/H64A variant (k_{NIR} = 49.8 $M^{-1}s^{-1}$; Phe43 is located at the CD1 position) [90]. The F43H mutant in contrast has much lower activity (k_{NIR} = 1.4 $M^{-1}s^{-1}$) [90]. This shows that the nitrite reductase results from an intricate interplay of different effects, of which the stabilization of the nitrite ligand by ArgE10 in the absence of an H-bonding residue on position E7 is an important factor, but not the only factor. The EPR spectrum of NO-bound ferrous GLB-33GD shows similar conformational states as found for other nitrosylated globins (Figure 7).

Based on its localization and its sequence, GLB33 has been suggested to be a putative neuropeptide receptor in *C. elegans* [16]. Since binding of nitrite requires a movement of the Arg residue into the distal haem pocket, the concomitant change of the globin structure may act as sensor, but future work on the full-length globin is needed to support this.

Acknowledgement

SVD acknowledges funding by the Research Foundation Flanders (FWO) (grant number G0C3518N). The authors thank the UAntwerp Research Council for funding via the BOF concerted research action '4D protein structure'. This work is dedicated to Sylvia Dewilde who was strongly involved in the first stage of this project and sadly passed away at the age of 47 on October 3th 2020.

Author contribution

Niels Van Brempt – Formal analysis, Investigation, Writing – Original Draft, Writing – Review & Editing
Roberta Sgammato - Investigation, Formal analysis, Writing – Original Draft, Writing – Review & Editing
Quinten Beirinckx – Investigation, Formal analysis, Writing – Review & Editing
Dietmar Hammerschmid – Investigation, Formal analysis, Writing – Oiginal Draft, Writing – Review & Editing
Frank Sobott - Writing – Review & Editing, Supervision
Sylvia Dewilde – Conceptualization, Supervision, Funding Acquisition
Luc Moens - Supervision, Writing – Review & Editing
Wouter Herrebout - Supervision, Writing – Review & Editing
Christian Johannessen – Supervision, Writing – Review & Editing,
Sabine Van Doorslaer – Conceptualization, Investigation, Formal analysis, Writing – Original Draft, Writing – Review & Editing, Supervision, Funding Acquisition;

References

1. S. N. Vinogradov, L. Moens, Diversity of globin function: enzymatic, transport, storage, and sensing, J. Biol. Chem. 283 (2008) 8773-8777. https://doi.org/10.1074/jbc.R700029200.
2. S. N. Vinogradov, D. Hoogewijs, X. Bailly, R. Arredondo-Peter, M. Guertin, J. Gough, S. Dewilde, L.Moens, J.R. Vanfleteren, Three globin lineages belonging to two structural classes in genomes from the three kingdoms of life. Proc. Natl. Acad. Sci. U.S.A., 102 (2005) 11385–11389. https://doi.org/10.1073/pnas.0502103102.
3. A. Pesce, M. Bolognesi, A. Bocedi, P. Ascenzi, S. Dewilde, L. Moens, T. Hankeln, T. Burmester, Neuroglobin and cytoglobin. Fresh blood for the vertebrate globin family, EMBO Rep. 3 (2002) 1146-1151. https://doi.org/10.1093/embo-reports/kvf248.
4. H. Wajcman, L. Kiger and M. C. Marden, C. R. Structure and function evolution in the superfamily of globins, C. R. Biol. 332, (2009) 273-282. https://doi.org/10.1016/j.crvi.2008.07.026.

5. S.N. Vinogradov, M. Tinajero-Trejo, R.K. Poole, D. Hoogewijs, Bacterial and archaeal globins - a revised perspective, Biochim. Biophys. Acta, 1834 (2013) 1789-1800. https://doi.org/10.1016/j.bbapap.2013.03.021.
6. A. Pesce, M. Nardini, M. Milani, M. Bolognesi, Protein structure in the truncated (2/2) hemoglobin family, IUBMB Life 59 (2007) 535-541. https://doi.org/10.1080/15216540701225933.
7. D. Hoogewijs, E. Geuens, S. Dewilde, L. Moens, A. Vierstraete, S. Vinogradov, J. R. Vanfleteren. Genome-wide analysis of the globin gene family of *C. elegans*. *IUBMB Life*, 56 (2004) 697–702. https://doi.org/10.1080/15216540500037562.
8. D. Hoogewijs, E. Geuens, S. Dewilde, A. Vierstraete, L. Moens, S. Vinogradov, J. R Vanfleteren. Wide diversity in structure and expression profiles among members of the *Caenorhabditis elegan*s globin protein family. *BMC genomics*, 8 (2007) 356. https://doi.org/10.1186/1471-2164-8-356.
9. E. Geuens, D. Hoogewijs, M. Nardini, E. Vinck, A. Pesce, L. Kiger, A. Fago, L. Tilleman, S. De Henau, M.C. Marden, R.E. Weber, S. Van Doorslaer, J. Vanfleteren, L. Moens, M. Bolognesi, S. Dewilde, Globin-like proteins in *Caenorhabditis elegans*: in vivo localization, ligand binding and structural properties, BMC Biochem. 11 (2010) 17. https://doi.org/10.1186/1471-2091-11-17.
10. L. Tilleman, F. Germani, S. De Henau, E. Geuens, D. Hoogewijs, B. P. Braeckman, J. R. Vanfleteren, L. Moens, S. Dewilde. Globins in *Caenorhabditis elegans*. IUBMB Life, 63 (2011) 166–174. https://doi.org/10.1002/iub.443.
11. A. Persson, E. Gross, P. Laurent, K.E. Busch, H. Bretes, M. De Bono. Natural variation in a neural globin tunes oxygen sensing in wild *Caenorhabditis elegans*. Nature, 458 (2009) 1030–1033. https://doi.org/10.1038/nature07820
12. S. De Henau, L. Tilleman, M. Vangheel, E. Luyckx, S. Trashin, M. Pauwels, F. Germani, C. Vlaeminck, J. R. Vanfleteren, W. Bert, A. Pesce, M. Nardini, M. Bolognesi, K. De Wael, L. Moens, S. Dewilde, B. P. Braeckman. A redox signalling globin is essential for reproduction in *Caenorhabditis elegans*. Nat. Commun., 6 (2015) 1–14. https://doi.org/10.1038/ncomms9782.
13. L. Tilleman, S. De Henau, M. Pauwels, N. Nagy, I. Pintelon, B, P. Braeckman, K, De Wael, S. Van Doorslaer, D. Adriaensen, J.P .Timmermans, L. Moens, S. Dewilde. An N-Myristoylated Globin with a Redox-Sensing Function That Regulates the Defecation Cycle in *Caenorhabditis elegans*. PLoS One, 7 (2012) 1–9. https://doi.org/10.1371/journal.pone.0048768.
14. C. Ren, Y. Li, R.g Han, Da. Gao, W. Li, J. Shi, D. Hoogewijs, B. P. Braeckman, S. De Henau, Y. Lu, W. Qu, Y. Gao, Y. Wu, Z. Li, H. Liu, Z. Wang, C. Zhang. GLB-13 is associated with oxidative stress resistance in *Caenorhabditis elegans*. IUBMB Life, 65(5) (2013) 423–434,. https://doi.org/10.1002/iub.1132.
15. Z. Hafideddine, T. Loier, N. Van Brempt, S. De Henau, H. Y. V. Ching, S. Neukermans, S. Defossé, H. Berghmans, R. Sgammato, R. Aerts, D. Hammerschmid, R. Moons, T. Bruegelmans, F. Sobott, C. Johannessen, W. Herrebout, B. P. Braeckman, L. Moens, S. Dewilde, S. Van Doorslaer, GLB-3: A resilient, cysteine-rich, membrane-tethered globin expressed in the reproductive and nervous system of Caenorhabditis elegans, J. Inorg. Biochem., 238 (2023) 112063 https://doi.org/10.1016/j.jinorgbio.2022.112063
16. L. Tilleman, F. Germani, S. De Henau, S. Helbo, F. Desmet, H. Berghmans, S. Van Doorslaer, D. Hoogewijs, L. Schoofs, B.P. Braeckman, L. Moens, A. Fago, S. Dewilde,

A globin domain in a neuronal transmembrane receptor of *Caenorhabditis elegans* and *Ascaris suu*m: molecular modeling and functional properties, J. Biol. Chem. 290 (2015) 10336–10352. https://doi.org/10.1074/jbc.M114.576520.
17. F. P. Nicoletti, E. Droghetti, B. D. Howes, J. P. Bustamante, A. Bonamore, N. Sciamanna, D. A. Estrin, A. Feis, A. Boffi, G. Smulevich, H-Bonding Networks of the Distal Residues and Water Molecules in the Active Site of Thermobifida Fusca Hemoglobin, Biochim. Biophys. Acta - Proteins Proteomics 1834 (2013), 1901–1909. https://doi.org/10.1016/j.bbapap.2013.02.033.
18. J. Qin, U. Pande, G.N. La Mar, F. Ascoli, P. Ascenzi, F. Cutruzzola, C. Travaglini-Allocatelli, M. Brunori, 1H NMR Study of the Dynamics of the PH Modulation of Axial Coordination in Aplysia Limacina (Val(E7)) and Sperm Whale Double Mutant His(E7→Val,Thr(E10)→Arg Metmyoglobin. J Biol Chem 268 (1993) 24012–24021.
19. M.T. Gladwin, A. N. Schechter, D. B. Kim-Shapiro, R. P. Patel, N. Hogg, S. Shiva, R. O. Cannon III, M. Kelm, D. A. Wink M. G. Espay, E H. Oldfield, R. M. Pluta, B. A. Freeman, J. R. Lancaster Jr., M. Feelisch, J. O. Lundberg, The emerging biology of the nitrite anion, Nature Chem. Biol. 6 (2005) 308-314. https://doi.org/10.1038/nchembio1105-308.
20. L. B. Maia, J. J. Moura, How Biology handles Nitrite. Chem. Rev. 114 (2014) 5273-5357. https://doi.org/10.1021/cr400518y
21. N. Castiglione, S. Rinaldo, G. Giardina, V. Stelitano, F. Cutruzzolà, Nitrite and Nitrite Reductases: From Molecular Mechanisms to Significance in Human Health and Disease, Antioxid. Redox Signal. 17 (2012) 684-716. https://www.liebertpub.com/doi/10.1089/ars.2011.4196
22. K. Cosby, K. S.Partovi, J. H. Crawford, R. P. Patel, C. D. Reiter, S. Martyr, B. K. Yang, M. A. Waclawiw, G. Zalos, X. Xu, K.T. Huang, H. Shields, D. B. Kim-Shapiro, A. N. Schechter, R. O. Cannon III, M. T. Nitrite Reduction to Nitric Oxide by Deoxyhemoglobin Vasodilates the Human Circulation. Nat. Med. 9 (2003), 1498–1505. https://doi.org/10.1038/nm954.
23. J. W. Jacklet, Nitric Oxide Signaling in Invertebrates. Invertebr. Neurosci. 3 (1997), 1–14. https://doi.org/10.1007/BF02481710.
24. U. Kreutzer, T. Jue, Role of Myoglobin as a Scavenger of Cellular NO in Myocardium. Am. J. Physiol. - Heart Circ. Physiol. 286 (2004) H985-991. https://doi.org/10.1152/ajpheart.00115.2003.
25. M.T. Gladwin, D. B. Kim-Shapiro, The Functional Nitrite Reductase Activity of the Heme-Globins. Blood 112 (2008), 2636–2647. https://doi.org/10.1182/blood-2008-01-115261.
26. D.D. Thomas K. M. Miranda, C. A. Colton, D. Citrin, M. G. Espey, D. A Wink, Heme proteins and nitric oxide (NO): the neglected, eloquent chemistry in NO redox signaling and regulation, Antioxid. Redox Signal. 5 (2003) 307-317. https://doi.org/10.1089/152308603322110887.
27. D. B. Kim-Shapiro, M.T. Gladwin, R. P. Patelc, N. Hogg, N. The Reaction between Nitrite and Hemoglobin: The Role of Nitrite in Hemoglobin-mediated Hypoxic Vasodilation. In: A. Gosh (Ed.) The Smallest Biomolecules: Diatomics and their Interactions with Heme Proteins; Elsevier, Amsterdam, 2008; p 269-289. https://doi.org/10.1016/B978-0-444-52839-1.X5001-3

28. J. B. Fox, J. S. Tomson, J. S. Thomson, The Formation of Green Heme Pigments from Metmyoglobin and Methemoglobin by the Action of Nitrite. Biochemistry 1964, 3 (9), 1323–1328. https://doi.org/10.1021/bi00897a023.
29. L. L. Bondoc, R. Timkovich, Structural Characterization of Nitrimyoglobin. J. Biol. Chem. 1989, 264 (11), 6134–6145. https://doi.org/10.1016/S0021-9258(18)83323-3.
30. A. Ioannou, A. Lambrou, V. Daskalakis, E. Pinakoulaki, Coupling of Helix E-F Motion with the O-Nitrito and 2-Nitrovinyl Coordination in Myoglobin. Biophys. Chem. 2017, 221, 10–16. https://doi.org/10.1016/j.bpc.2016.11.009.
31. L. Capece, L. Boechi, L. L. Perissinotti, P. Arroyo-Mañez, D. E. Bikiel, G. Smulevich, M. A. Marti, D. A. Estrin, Small Ligand-Globin Interactions: Reviewing Lessons Derived from Computer Simulation. Biochim. Biophys. Acta - Proteins Proteomics 1834 (2013) 1722–1738. https://doi.org/10.1016/j.bbapap.2013.02.038.
32. I. Serra, D. Schmidt, V. Pfanzagl, G. Mlynek, S. Hofbauer, K. Djinović- Carugo, P. G. Furtmüller, I. García-Rubio, S. Van Doorslaer, C. Obinger, Impact of the dynamics of the catalytic arginine on nitrite and chlorite biding by dimeric chlorite dismutase, J. Inorg. Biochem. 227 (2022) 111689. https://doi.org/10.1016/j.jinorgbio.2021.111689.
33. J. W. A. Allen, C. W. Higham, R. S. Zajicek, N. J. Watmough, S.J. Ferguson, A Novel, Kinetically Stable, Catalytically Active, All-Ferric, Nitrite-Bound Complex of Paracoccus Pantotrophus Cytochrome Cd1. Biochem. J. 366 (2002), 883–888. https://doi.org/10.1042/BJ20020795.
34. E.P. Day, J. Peterson, J.J. Bonvoisin, L. J. Young, J.O. Wilkerson, L.M. Siegel, Magnetization of the Sulfite and Nitrite Complexes of Oxidized Sulfite and Nitrite Reductases: EPR Silent Spin S = 1/2 States. Biochemistry, 27 (1988), 2126–2132. https://doi.org/10.1021/bi00406a04.
35. S. Van Doorslaer, Understanding Heme Proteins with Hyperfine Spectroscopy, J. Magn. Reson. 280 (2017) 79–88. https://doi.org/10.1016/j.jmr.2017.01.008.
36. T. G. Spiro, G. Smulevich, C. Su, Probing Protein Structure and Dynamics with Resonance Raman Spectroscopy: Cytochrome c Peroxidase and Hemoglobin, Biochemistry 29 (1990), 4497–4508. https://doi.org/10.1021/bi00471a001.
37. R. Sgammato, W. Herrebout, C. Johannessen, Resonance Raman Optical activity of the Imidazole-Myoglobin Complex: Titrating Enhancement, J. Raman Spectrosc. 50 (2019) 1905-1913. https://doi.org/10.1002/jrs.5735.
38. S. Dewilde, K. Mees, L. Kiger, C. Lechauve, M.C. Marden, A. Pesce, M. Bolognesi, L. Moens, Expression, Purification, and Crystallization of Neuro- and Cytoglobin. Methods Enzymol. 436 (2008) 341–357. https://doi.org/10.1016/S0076-6879(08)36019-4.
39. P. H. C. Eilers, A perfect smoother. Anal. Chem. 75 (2003), 3631–3636. https://doi.org/10.1021/ac034173t.
40. A. Schweiger, G. Jeschke, Principles of pulse electron paramagnetic resonance, Oxford University Press, New York (2001).
41. P. Höfer, A. Grupp, H. Nebenführ, M. Mehring, Hyperfine sublevel correlation (HYSCORE) spectroscopy: a 2D ESR investigation of the squaric acid radical, Chem. Phys. Lett. 132 (1986) 279–282. https://doi.org/10.1016/0009-2614(86)80124-5.
42. S. Stoll, A. Schweiger, EasySpin, a comprehensive software package for spectral simulation and analysis in EPR, J. Magn. Reson. 178 (2006) 42–55. https://doi.org/10.1016/J.JMR.2005.08.013.

43. J. Yi, J. Heinecke, H. Tan, P.C. Ford, G. B. Richter-Addo, The distal pocket histidine residue in horse heart myoglobin directs the O-binden mode of nitrite to the heme iron, J. Am. Chem. Soc. 131 (2009) 18119-18128. https://doi.org/10.1021/ja904726q
44. M. Nagai, C. Kobayashi, Y. Nagai, K. Imai, N. Mizusawa, H. Sakura, S. Neya, M. Kayanuma, M. Shoji, S. Nagatomo, Involvement of propionate side chains of the heme in circular dichroism of myoglobin: Experimental and theoretical analyses, J. Phys. Chem. B 119 (2015) 1275-1287. https://doi.org/10.1021/jp5086203.
45. M. Nagai, Y. Nagai, K. Imai, S. Neya, Circular dichroism of hemoglobin and myoglobin, Chirality 26 (2014) 438-442. https://doi.org/10.1002/chir.22273
46. M. Nagai, Y. Nagai, Y. Aki, K. Imai, Y. Wada, S. Nagatomo, Y. Yamamoto, Effect of reversed heme orientation on circular dichroism and cooperative oxygen binding of human adult hemoglobin, Biochemistry 47 (2008) 517-525. https://doi.org/10.1021/bi7015519
47. R. Schweitzer-Stenner, Cytochrome c: A multfunctional protein combining onformational rigidity with Flexibility, New J. Sci (2014) 484538. https://doi.org/10.1155/2014/484538.
48. T.-J. Shen, N. T. Ho, V. Simplaceanu, M. Zou, B. N. Green, M. F. Tam, C. Ho, Production of unmodified human adult haemoglobin in Escherichia coli, Proc. Natl. Acad. Sci. USA, 90 (1993) 8108-8112. https://doi.org/10.1073/pnas.90.17.8108.
49. A. Feis, B. D. Howes, L. Milazzo, D. Coppola, G. Smulevich, Structural Determinants of Ligand Binding in Truncated Hemoglobins: Resonance Raman Spectroscopy of the Native States and Their Carbon Monoxide and Hydroxide Complexes. *Biopolymers*. 109 (2018) e23114. https://doi.org/10.1002/bip.23114.
50. A. I. Ioanitescu, S. Dewilde, L. Kiger, M. C. Marden, L. Moens, S. Van Doorslaer, Characterization of Nonsymbiotic Tomato Hemoglobin. Biophys. J. 89 (2005), 2628–2639. https://doi.org/10.1529/biophysj.105.060582.
51. A. Feis, M.P. Marzocchi, M. Paoli, G. Smulevich, Spin State and Axial Ligand Bonding in the Hydroxide Complexes of Metmyoglobin, Methemoglobin, and Horseradish Peroxidase at Room and Low Temperatures. Biochemistry 33 (1994), 4577–4583. https://doi.org/10.1021/bi00181a019.
52. F. P. Nicoletti, E. Droghetti, B. D. Howes, J. P. Bustamante, A. Bonamore, N. Sciamanna, D. A. Estrin, A. Feis, A. Boffi, G. Smulevich, Interplay of H-bond donor-acceptor role of the distal residues in hydroxyl ligand stabilization of Thermobifida fusca truncated hemoglobin, Biochemistry 53 (2014) 8021-8030. https://doi.org/10.1021/bi501132a.
53. C.P. Scholes, R.A. Isaacson, G. Feber, Determination of the zero-field splitting of Fe3+ in heme proteins from the temperature dependence of the spin-lattice relaxation rate, Biohim. Biophys. Acta 244 (1971) 206-210. https://doi.org/10.1016/0304-4165(71)90138-3.
54. D. W. Kraus, J. B. Wittenberg, Hemoglobins of the Lucina Pectinata/Bacteria Symbiosis. II. An electron paramagnetic resonance and optical sprectal study of the ferric proteins. J. Biol. Chem. 265 (1990), 16054–16059. https://doi.org/10.1016/S0021-9258(17)46186-2.
55. D. A. Svistunenko, B. J. Reeder, M. M. Wankasi, R.-L. Silaghi-Dumitrescu, C. E. Cooper, S. Rinaldo, F. Cutruzzolà, M. T. Wilson, Reaction of Aplysia limacina metmyoglobin with hydrogen peroxide, Dalton Trans. (2007) 840. https://doi.org/10.1039/B615770J

56. D. B. Nye. E. A. Johnson, M. H. Ma, J. T. J. Lecomte. Replacement of the heme axial lysine as a test of conformational adaptability in the truncated hemoglobin THB1, J. Inorg. Biol. 201 (2019) 110824. https://doi.org/10.1016/j.jinorgbio.2019.110824.
57. Z. N. Nilsson, B. L. Mandella, K. Sen, D. Kekilli, M. A. Hough, P. Moënne-Loccoz, R. W. Strange, and C. R. Andrew. Distinguishing Nitro vs Nitrito Coordination in Cytochrome c Using Vibrational Spectroscopy and Density Functional Theory. Inorg. Chem. 56 (2017) 13205–13213. https://doi.org/10.1021/acs.inorgchem.7b01945.
58. B. Wang, Y. Shi, J. Tejero, S. M. Powell, L. M. Thomas, M. T. Gladwin, S Shiva, Y. Zhang, G. B. Richter-Addo, Nitrosyl Myoglobins and Their Nitrite Precursors: Crystal Structural and Quantum Mechanics and Molecular Mechanics Theoretical Investigations of Preferred Fe -NO Ligand Orientations in Myoglobin Distal Pockets. Biochemistry *57* (2018) 4788–480. https://doi.org/10.1021/acs.biochem.8b00542.
59. J. Navascués, C. Perez-Rontome, M. Gay, M. Marcos, F. Yang, F. A . Walker, A. Desbois, J. Abian, M. Becana, Leghemoglobin Green Derivatives with Nitrated Hemes Evidence Production of Highly Reactive Nitrogen Species during Aging of Legume Nodules. Proc. Natl. Acad. Sci. 109 (2012), 2660–2665. https://doi.org/10.1073/pnas.111655910.
60. W. Tse, N. Whitmore, M. R. Cheesman, N. J. Watmough, Influence of the heme distal pocket on nitrite binding orientation and reactivity in sperm whale myoglobin, Biochem. J. 478 (2021) 927-942. https://doi.org/10.1042/BCJ20200596.
61. D. E. Schwab, J. S. Stamler, D. J. Singel, EPR Spectroscopy of Nitrite Complexes of Methemoglobin. Inorg. Chem. 49 (2010), 6330–6337. https://doi.org/10.1021/ic902085s.
62. C. He, H. Ogata, W, Lubitz, Elucidation of the Heme Active Site Electronic Structure Affecting the Unprecedented Nitrite Dismutase Activity of the Ferriheme b Proteins, the Nitrophorins. Chem. Sci. 7 (2016), 5332–5340. https://doi.org/10.1039/c6sc01019a.
63. P. L. Hagedoorn, D. C. de Geus, W. R. Hagen, Spectroscopic characterization and ligand-binding properties of chlorite dismutase from the chlorate respiring bacterial strain GR-1, FEBS J. 269 (2002) 4905-4911 https://doi.org/10.1046/j.1432-1033.2002.03208.x.
64. A. C. Leney, A. J. R. Heck, Native Mass Spectrometry: What is in the Name? J. Am. Soc. Mass Spectrom. 28 (2017) 5-13. https://doi.org/10.1007/s13361-016-1545-3
65. H. Hernández, C. V. Robinson, Determining the stoichiometry and interactions of macromolecular addemblies from mass spectrometry, Nat. Prot. 2 (2007) 715-726. https://doi.org/10.1038/nprot.2007.73
66. J. Gault, J. A. C. Donlan, I. Liko, J. T. S. Hopper, K. Gupta, N. G. Housden, W. B. Struwe, M. T. Marty, T. Mize, C. Bechara, Y. Zhu, B. Wu, C. Kleanthous, M Belov, E. Damoc, A. Makarov, C. V. Robinson, High-resolution mass spectrometry of small molecules bound to membrane proteins, Nat. Methods 13 (2016) 333-336. https://doi.org/10.1038/nmeth.3771
67. F. Sobott, M. G. McCammon, H. Hernández, C. V. Robinson, The flight of macromolecular complexes in a mass spectrometer, Philos. Trans. A Math. Phys. Eng. Sci., 363 (2005) 379-389. https://doi.org/10.1098/rsta.2004.1498
68. B. T. Ruotolo, C. V. Robinson, Aspects of native proteins are retained in vacuum, Curr. Opin. Chem. Biol. 10 (2006) 402-408. https://doi.org/10.1016/j.cbpa.2006.08.020
69. J. T. S. Hopper, N. J. Oldham, Collision Induced Unfolding of Protein Ions in the Gas Phase Studied by Ion Mobility-Mass Spectrometry: The Effect of Ligand Binding on

Conformational Stability. J. Am. Soc. Mass Spectrom. 20 (2006), 1851-1858 https://doi.org/10.1016/j.jasms.2009.06.010
70. A. Konijnenberg, A. Butterer, F. Sobott, Native ion mobility-mass spectrometry and related methods in structural biology. Biochim. Biophys. Acta, 1834 (2013) 1239–1256. https://doi.org/10.1016/j.bbapap.2012.11.013
71. B. I. Goetz, H. W. Shields, S. Basu, P. Wang, S. B. King, N. Hogg, M. T. Gladwin, D. B. Kim-Shapiro, An electron paramagnetic resonance study of the affinity of nitrite for methemoglobin, Nitric oxide, 22 (2010) 149-154 https://doi.org/10.1016/j.niox.2009.10.009.
72. C.P.S. Taylor, The EPR of low spin heme complexes relation of the τ2g hole model to the directional properties of the g tensor, and a new method for calculating the ligand field parameters, Biochim, Biophys Acta - Protein Struct. 491 (1977) 137–148 https://doi.org/10.1016/0005-2795(77)90049-6.
73. P.P. Schmidt, R. Kappl, J. Hüttermann, On the mode of hexacoordinated NO-binding to myo-and hemoglobin: Variable-temperature EPR studies at multiple microwave frequencies. Appl Magn Reson. 21 (2001) 423-440. https://doi.org/10.1007/BF03162418.
74. E. Wajnberg, M. P. Linhares, L. J. El-Jaick, G. Bemski Nitrosyl hemoglobin: EPR components at low temperatures. Eur. Biophys. J. 21 (1992) 57-61. https://doi.org/10.1007/BF00195444.
75. F. Trandafir, S. Van Doorslaer, S. Dewilde, L. Moens, Temperature dependence of NO binding modes in human neuroglobin. Biochim Biophys Acta (BBA)-Proteins Proteomics 1702 (2004) 153-161. https://doi.org/10.1016/j.bbapap.2004.08.004.
76. R. H. Morse, S.I. Chan, Electron paramagnetic resonance studies of nitrosyl ferrous heme complexes. Determination of an equilibrium between two conformations. J. Biol. Chem. 255 (1980) 7876-7882. https://doi.org/10.1016/S0021-9258(19)43916-1 .
77. A. Pesce, L. Thijs, M. Nardini, F. Desmet, L. Sisinni, L. Gourlay, A. Bolli, M. Coletta, S. Van Doorslaer, X. Wan, M. Alam, P. Ascenzi, L. Moens, M. Bolognesi, S. Dewilde, HisE11 and HisF8 provide bis-histidyl heme hexa-coordination in the globin domain of Geobacter sulfurreducens Globin-coupled sensor, J. Mol. Biol. 386 (2009) 246-260. https://doi.org/10.1016/j.jmb.2008.12.023
78. I. I. Vlasova, V. A. Tyurin, A. A. Kapralov, I. V. Kurnikov, A. N. Osipov, M. V. Potapovich, D. A. Stoyanovsky, V. E. Kagan, Nitric oxide inhibits peroxidase activity of cytochrome c Cardiolipin complex and blocks cardiolipin oxidation, J. Biol. Chem. 281 (2006) 14554-14562. https://doi.org/10.1074/jbc.M509507200
79. M. Radoul, M. Sundararajan, A. Potapov, C. Riplinger, F. Neese, D. Goldfarb, Revisiting the nitrosyl complex of myoglobin by high-field pulse EPR spectroscopy and quantum mechanical calculations, Phys. Chem. Chem. Phys. 12 (2010) 7276-7289. DOI https://doi.org/10.1039/C000652A
80. D. Schmidt, I. Serra, G. Mlynek, V. Pfanzagl, S. Hofbauer, P. G. Furtmüller, K. Djinović-Carugo, S. Van Doorslaer, C. Obinger, Arresting the catalytic argenine in chlorite dismutases: Impact on heme coordination, thermal stability and catalysis, Biochemistry, 60 (2021) 621-634. https://dx.doi.org/10.1021/acs.biochem.0c00910
81. G. M. Giacometti, A. Da Ros, E. Anonini, M. Brunori, Equilibrium and kinetics of the reaction of Aplysia myoglobin with azide, Biochemistry 14 (1975) 1584-1588. https://doi.org/10.1021/bi00679a006

82. J. Qin, G. N. La Mar, F. Ascoli, M. Bolognesi, M. Brunori, Solution 1H Nuclear Magnetic Resonance Determination of Hydrogen Bonding of the E10 (66) Arg Side-chain to the bound ligand in Aplysia Cyano-met Myoglobin. J. Mol. Biol. 224 (1992) 891-897. https://doi.org/10.1016/0022-2836(92)90456-T
83. C. Travaglini Allocatelli, F. Cutruzzola, A. Brancaccio, M. Brunori, J. Qin, G. N. La Mar, Structural and functional characterization of sperm whale myoglobin mutants: Role of arginine (E10) in ligand stabilization. *Biochemistry* 32(1993) 6041-6049. https://doi.org/10.1021/bi00074a015
84. D. L. Rousseau, Y.-C. Ching, M. Brunori, G. M. Giacometti, Axial Coordination of Ferric Aplysia Myoglobin, J. Biol. Chem. 264 (1989) 7878-7881. https://doi.org/10.1016/S0021-9258(18)83125-8
85. M.R. Cheesman, G. Greenwood, A. J. Thomson, Magnetic circular dichroism of hemoproteins, Adv. Inorg. Chem. 36 (1991) 201-255. https://doi.org/10.1016/S0898-8838(08)60040-9
86. Y. Orii, M. Morita, Measurement of the pH of frozen buffer solutions by using pH indicators, J. Biochem. 81 (1977) 163-168. https://doi.org/10.1093/oxfordjournals.jbchem.a131431
87. M. Sundararajan, F. Neese, Distal Histidine Modulates the Unusual O-Binding of Nitrite to Myoglobin: Evidence from the Quantum Chemical Analysis of EPR Parameters. *Inorg Chem*. 54 (2015) 7209-7217. https://doi.org/10.1021/acs.inorgchem.5b00557.
88. A. Boffi, J. B. Wittenberg, E. Chiancone, Circular dichroism spectroscopy of Lucina I hemoglobin. FEBS Lett. 411(1997) 335-338. https://doi.org/10.1016/S0014-5793(97)00727-8.
89. V. S. Sharma, T. G. Traylor, R. Gardiner, H. Mizukami, Reaction of nitric oxide with heme proteins and model compounds of hemoglobin. Biochemistry 26 (1987) 3837-3843. https://doi.org/10.1021/bi00387a015
90. L.-B. Wu, H. Yuan, S.-Q Gao, Y. You, C.-M. Nie, G.-B. Wen, Y.-W. Lin, X. Tan, Regulating the reductase activity of myoglobin by redesinging the heme active center, Nitric Oxide 57 (2016) 21-29. https://doi.org/10.1016/j.niox.2016.04.007